THE VELOCITY FIELD DOWNSTREAM FROM A TWO-DIMENSIONAL MODEL HILL

PART 1

By
Erich J. Plate and Chi W. Lin

Part 1 of Final Report on Grant No. DA AMC-36-039-63-G7

CER65EJP14

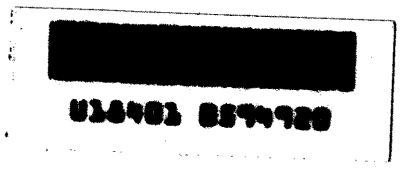

ACKNOWLEDGEMENTS

Dr. Alexander R. Craw, of the U. S. Army CBR Agency, Ft. Detrick, Maryland, and Dr. J. E. Cermak of Colorado State University provided encouragement and counsel throughout the study. Calvin Finn designed and tested the dual wire discriminator, and gave invaluable help throughout every phase of the experimental part. C. M. Sheih, S. Chowdhury and S. T. Lin, graduate students at Colorado State University, helped with the taking and analysis of data. To them, the writers wish to express their gratitude.

TABLE OF CONTENTS

LIST OF FIGURES

LIST OF TABLES

THE VELOCITY FIELD DOWNSTREAM FROM A TWO-DIMENSIONAL MODEL HILL

1. INTRODUCTION

Many experimental investigations of the atmospheric surface layer and of the boundary layer along a flat plate in a wind tunnel have shown that both flows are similar, provided that the atmospheric profiles are taken over a flat terrain with a long and undisturbed fetch. Such a situation is, however, rather exceptional on the earth's surface, and obstructions in the wind path are the rule. Very little is known about the effect of a disturbance on boundary layer flows; neither wind tunnel data nor field data are available in sufficient quantity to deduce general model laws.

The effect of a disturbance is felt in the velocity field downwind in two ways. It shows in the mean velocity distribution which deviates from that on a smooth flat plate, but it influences even more strongly the turbulence structure, because any obstacle increases the amount of turbulence.

Both effects are of greatest significance if the spreading and distribution of a diffusion cloud is to be predicted. For describing the spreading of diffusing matter, one needs to know its mean convection, under the influence of the local mean velocities, and also the rate of spreading, or dispersion under the influence of the turbulence. A description of the effect of an obstacle on diffusion therefore requires a knowledge, of either theoretical or experimental nature, of the mean and the turbulent velocity field.

As is well known, a solution of the equations for turbulent boundary layer flows is as yet not available. Even less hope exists for the case where the boundary layer is disturbed by an obstacle. It is unlikely that reasonable models which permit prediction of mean velocity profiles and the structure of turbulence are forthcoming in the near future, unless guided by experimental evidence - which does as yet exist only in rare cases. Therefore, the first step in solving problems of diffusion in disturbed boundary layers must be an experimental program, which will

establish general trends and relations between the pertinent variables. Information obtained through such an experimental program serves as a guide line for future experiments, or as proving stone on which any theoretical model must be tested. In any event, data obtained can be used for developing model laws, which may permit modeling a complicated situation for which an analytical description cannot be given.

Among the possible types of obstacles the two-dimensional hill appeared the most suitable for trying to establish model laws. The flow generated by an infinitely long obstruction placed perpendicular to the flow has the advantage of being approximately two-dimensional. It also has the advantage that many natural obstacles, like hills, dams, shelter strips, etc., exhibit similar configurations. It is for these reasons that two-dimensional hills were chosen as a first approach toward a study of disturbed boundary layers.

In order to cover a wide variety of variables which govern the geometry of the hill model, two basic model types were used. Type one consisted of a wedge, with a vertical front facing the flow and a wedged back. This model was chosen for maintaining a well defined separation line and permitting a simple geometrical description. The ratios of depth e to height h chosen were 1, 2, and 4, at two different heights of the model of 1 inch and 2 inches. Type two has the shape of a sine wave for angles between zero and π, with a base equal to 5 times the amplitude. Two heights of 2 inches and 4 inches were used. The hill models are shown in Fig. 1.

For the hill models, a variety of different ambient velocities were used, and data were obtained for the flow cases listed in Table 1.

In this report, a systematic presentation will be given of the velocity and turbulence data which were obtained downstream from the two-dimensional model hills. The data are analyzed following procedures which are considered applicable to the flow situation, and tentative results of analysis are presented.

TABLE 1

T_p = temperature of plate

T_a = temperature of ambient air

Hill	Model Shape	Velocity (fps)	Wind Tunnel	Thermal Case	T_p °F	T_a °F	Turbulence Data
1"x 4"	Wedge	30	Small	No			No
	"	60	Small	No			No
2"x 2"	Wedge	15	Small	No			No
	"	30	Small	No			Yes
	"	60	Small	No			Yes
2"x 4"	Wedge	15	Small	No			No
	"	30	Small	No			Yes
	"	60	Small	No			Yes
	"	15	Big	No			No
	"	30	Big	No			Yes
	"	60	Big	No			No
	"	30	Big	Yes	300	72	No*
	"	60	Big	Yes	300	72	No*
2"x 8"	Wedge	30	Small	No			Yes
	"	60	Small	No			No
2"x 10"	Sinusoidal	30	Small	No			No
	"	30	Big	No			Yes
	"	60	Big	No			No
4"x 20"	Sinusoidal	15	Big	No			No
	"	30	Big	No			Yes
	"	60	Big	No			No
	"	30	Big	Yes	300°F	50°F	No*
	"	60	Big	Yes	300°F	50°F	No*

* The results of these experiments have not yet been analyzed and are not discussed in this report.

2. EXPERIMENTAL EQUIPMENT AND PROCEDURES

Experiments were performed in the wind tunnels of the Fluid Dynamics and Diffusion Laboratory of Colorado State University. The instruments used were part of the standard laboratory equipment with the exception of one instrument which was built for the purpose of determining the location of stagnation points in turbulent flows. The wind tunnels and the instrumentation are briefly described.

2.1 The Wind Tunnels

The bulk of the data, corresponding to a low boundary layer thickness in the undisturbed flow, were taken in the small low speed wind tunnel shown in Fig. 2. The wind tunnel has a test section with a useable length of 30 ft and a cross sectional area of 6 x 6 ft^2. Models were placed on the floor at a distance of 14 ft from the wind tunnel entrance. The boundary layer upstream from the model was artificially thickened by a roughened section of the floor at the wind tunnel entrance. A trip fence consisting of a strip of 1/2" saw teeth was followed by a 14" long strip of 1/4" gravel. This arrangement assured a turbulent boundary layer at the model.

The air speed in the low speed wind tunnel was controlled with a constant speed, variable pitch fan. Velocities of 15, 30, 45 and 60 fps were used. The pressure gradient of the tunnel was approximately zero, at 30 fps, but no corrections were made after installation of the models. Instead, pressures were measured along the center line of the wind tunnel floor for each model and at each ambient velocity. The measurements were made by means of static pressure taps which were embedded into the wind tunnel floor at the intervals shown in Fig. 2.

Data for the models embedded into a thick boundary layer were taken in the Meteorological Wind Tunnel of the U. S. Army. This facility is described by Plate and Cermak (7). This tunnel is equipped with a boundary layer trip consisting of heavy saw tooth fences followed by a 4 ft section of 3/8" gravel fastened all around the exit portion of the

transition section (see Fig. 3). The models were placed at a distance of 40 ft downstream from the tunnel entrance, in front of the beginning of the temperature controlled surface. No pressure measurements could be taken along the floor of this wind tunnel; the only pressure measurements were taken around the models.

The speed of the air in the Army Meteorological Wind Tunnel is controlled with a variable speed, variable pitch aircraft propellor. The temperature of the ambient air is maintained at a constant level by means of an air conditioning system.

2.2 Instrumentation

The measured quantities consisted of pressures, mean velocities, turbulent velocity components and their spectra, turbulent shear stresses, and the location of the point of reattachment of the separation stream line downstream from the hill model.

2.21 Pressure Measurements

Pressures were measured around the models, along the floor, and for some cases inside the flow. For measuring pressures around the model, pressure taps consisting of 1/16" holes at intervals shown in Fig. 1 were arranged on the models. The pressure taps were connected through plastic tubing to an electronic manometer (Transonics Equibar 120) where they measured against a suitable reference pressure. The reference pressure for all experiments was the pressure of a wall tap located at a large distance downstream from the model, as indicated in Figs. 2 and 3. The floor pressures were measured by using 1/16" holes in the floor. The pressure inside the flow was measured with the static pressure holes of a pitot static tube. These pressures were measured continuously by using a probe positioner which was driven by a small motor. A potentiometer geared to the guide bar of the positioner gave a voltage drop proportional to the distance from the floor which was applied to the x-axis of an x-y recorder (Type Moseley 135). The d-c output proportional to the

relative pressure from the electronic manometer (Type Transonic Equibar 120) was plotted on the y-axis of the recorder. The electronic manometer was, in regular intervals, calibrated against the reading of a water micromanometer (Flow Corporation Type MM-2), but the stability of the electronic manometer was so good that adjustments were hardly ever necessary. The pressure measuring instrumentation is shown in Fig. 4.

2.22 Velocity Measurements

Mean velocities were measured with a pitot static tube arranged in the same manner as the pressure measuring devices. From knowledge of the dynamic pressure, the barometric pressure, and the temperature, the velocities could be calculated.

Turbulent velocity components were measured with hot wire equipment. Most of the time only turbulent intensities were measured with a single platinum hot wire of a diameter of 0.0001 inches, a length of 0.1 inches, and a cold resistance of approximately 5 Ohms. The hot-wire probe was made by the DISA Co., with the wires mounted by laboratory technicians. Turbulent intensity profiles were obtained by placing the hot-wire probe on the probe positioner used for measuring the pressure and velocity profiles. The hot-wire probe was operated by a constant temperature type servo amplifier Type Hubbard 3A. The AC output of this instrument was fed into a true rms-meter Type Bruel and Kjaer 2409. This instrument had been modified to give an output voltage which is proportional to the meter reading. This voltage and the voltage proportional to the probe position were applied to the two axes of the x-y recorder, and continuous intensity profiles were obtained. The arrangement is shown in Fig. 5. The Hubbard hot-wire amplifier gives an output voltage which is a linear function of the velocity. The function is determined by calibrating the d-c meter of the amplifier against the pitot static tube in the free stream of the wind

tunnel. With the slope of the calibration curve a constant, the plotted profiles can conveniently be converted into the intensity readings by multiplying data points with a constant factor.

For some cases it was desired to obtain energy spectra of the turbulent intensities, turbulent shear data, or data on the fluctuating velocity in the vertical direction. For this purpose, recordings were made of single or crossed hot-wire outputs as a function of time at a given point. The recordings were made on magnetic tape, by placing an impedance matching and attenuating stage between the Hubbard amplifier output and the magnetic tape recorder (Mincom Type C-100) . The data were evaluated with the analog computing equipment of Colorado State University. The equipment is shown schematically in Fig. 6.

2.23 Measuring the Distance of the Reattachment Point from the Hill Crest

For measuring the reattachment point downstream from the model hill, a special technique was required. Since substantial turbulence exists near the reattachment point (which is of course a result of the separation on the model crest), the condition that the mean velocity at reattachment is equal to zero cannot be used because a hot-wire anemometer measures, in the absence of mean velocities, the turbulent rms value, and a zero velocity point cannot well be defined by moving the hot-wire anemometer along the floor. The same is true for heat transfer shear measurements. Techniques which have been used with some success involve flow visualization with oil film techniques, or with smoke - techniques which do not permit very accurate results for highly turbulent flow. Therefore, the following reasoning was used to design a more reliable device. Very near the wall, on the reattachment stream line, the mean horizontal velocity is equal to zero, so that the hot-wire anemometer measures only the turbulence present at that location. The assumption can be made that the turbulent velocity component parallel

to the wall is homogeneous, i. e. velocities of a given magnitude are equally likely to occur directed upstream as directed downstream. Thus, if a hot wire could be made that "sees" velocity components in one direction only, it would in this homogeneous turbulence, in the absence of mean velocities, measure some velocity only 50 per cent of the time. During the other 50 per cent of the time, the direction would be opposite, and this special wire would not measure anything. A hot-wire probe which behaves like this special wire was designed by using an idea which was advanced by Man Moon (4). Two hot wires of exactly the same length and resistance were placed parallel and so close together as was possible without touching. Each one was operated on by one of the two channels of the Hubbard hot-wire anemometer amplifier. The outputs of the hot-wire amplifiers are fed into a special discriminating circuit shown in Fig. 7. The discriminating circuit provides a train of 100, 000 pulses per second as long as the input to one preset channel (channel A) of the discriminator is larger than the input to the other channel (channel B). If the input into channel B is larger, then no signal is generated by the circuit.

Now if the two wire probe is placed at some suitable distance above the floor with the plane through the axes of the wires parallel to the floor, then, when the flow velocity is parallel to the floor, the downstream wire is in the wake of the upstream wire and consequently does not get cooled as much as the upstream wire. Under these conditions, the feedback amplifier would give a larger current output for the wire located upstream than for the downstream wire. If the signals from the two wires are fed into the discriminating circuit, the circuit would give an output which indicates on a pulse counter, (Hewlett Packard Type 522) which percentage of time the one wire yields a larger signal than the other. If the initial set up has been such that each wire had the larger signal one half of the time - which was obtained by placing the two wires parallel to the direction of the mean flow and adjusting the attenuators of the discriminator - then the 50 per cent reading of the discriminator circuit in an unknown flow

would correspond to the homogeneous turbulence location, which yielded the reattachment point. The arrangement of the probe is shown in Fig. 8, and the equipment used is shown in Fig. 9.

3. DATA ANALYSIS

In this chapter, the basic question of modeling a two-dimensional hill in a wind tunnel is treated. The conditions are first indicated under which modeling is possible, and then the various assumptions are tested on which the modeling criteria are based. The investigation yields very satisfactory agreement between assumptions and experimental results for the velocity distributions at large distances downstream from the hill, but no final conclusions can be drawn as yet for the important flow in the standing eddy region directly downstream of the model.

3.1 Modeling of a Two-Dimensional Hill

The purpose of this study was to obtain model laws which permit the scaling of natural boundary layer flows with obstructions in a wind tunnel environment. It does not seem suitable to derive the modeling parameters by applying an inspectional analysis to the Navier Stokes equations directly, but a similar procedure is possible. Plate (8) has shown that, in the absence of pressure gradients in the direction of flow, the momentum balance of the disturbed boundary layer can be expressed by a momentum equation of the form:

$$\frac{\theta(x)}{\delta_c} = \frac{\theta_o}{\delta_o} + 1/2\, C_D \frac{h}{\delta_o} + \frac{h}{\delta_o} \int_{x_a/h}^{x/h} c_f\,(x/h)\; d\,(x/h) \quad . \tag{3-1}$$

In this equation, the momentum thickness θ is defined as

$$\theta = \int_0^{\delta} \frac{u}{u_a} \left(1 - \frac{u}{u_a}\right) dy \tag{3-2}$$

where u_a = ambient velocity in the potential core outside of the boundary layer and u is the horizontal velocity at a distance y from the floor.

Term 1 on the left is the ratio of the momentum thickness at some distance x downstream from the crest of the hill to the thickness of the boundary layer in the undisturbed flow (before the obstacle was placed into the flow) at the location of the crest of the model hill. Term 2 is the same ratio, but θ_o is defined as the momentum thickness of the undisturbed flow at $x = 0$. The second term on the right side, term 3, is the contribution of the drag of the model hill to the momentum balance. The drag coefficient C_D is defined as

$$D = C_D \cdot h \left(\frac{1}{2} \rho u_a^2 \right) \tag{3-3}$$

where D is the model hill drag per unit width, and h is the height of the model hill.

The remaining term 4 represents the contribution of the boundary friction to the momentum balance. Since directly downstream of an obstacle there usually exists a standing eddy region in which the velocity near the ground is directed towards the obstacle, the net contribution of the ground shear is, at some distance x_a dowstream from the model hill, equal to zero. Thus, only the ground shear downstream from this distance x_a is to be included. In the case of an obstacle consisting of a sharp edged fence, the distance x_a is of the order of $30 \cdot h$, while the values of c_f correspond to those that would be obtained at the same place along the flat plate forming the ground, if the boundary layer had remained undisturbed. Provided, then, that the flow downstream from a two-dimensional model hill essentially obeys the same laws as the flow downstream from a two-dimensional fence, modeling of the flow is achieved under the following conditions:

a. The velocity distribution in the undisturbed boundary layer must be similar for model and prototype. This condition is easily met in practical cases, since the wall law

$$\frac{u}{u_*} = \frac{1}{k} \ln \frac{y}{z_o} \tag{3-4}$$

holds both in the wind tunnel and in nature. In Eq. (3-4), u_* is the shear velocity $u_* = \frac{\sqrt{\tau_o}}{\rho}$, with τ_o the ground stress, and z_o is the roughness height. The shear velocity can be adjusted over a wide range of values by simply varying the mean velocity in the ambient air stream, and the roughness height z_o can be chosen by the selection of a suitable roughness material for the boundary. The ratio of the vertical length scales for model and prototype is then found as the ratio of the z_o values.

b. The drag coefficient of the model hill must be the same as that of the natural obstacle. A wide range of drag coefficients can be obtained by varying the stream-lining of the model hill. Thus, the modeling of the drag coefficients is mainly a problem of appropriately defining a coefficient in a natural flow. However, this question is not treated in the present report.

c. The ratio h/δ_o must be the same for both wind tunnel and prototype. Since δ_o is a quantity which is not defined, nor easily definable, in nature, one might tentatively define a ratio of $\frac{h}{\delta_o}$ by the following consideration. Assume that the velocity distribution over the height of an obstacle in the flow is to be similar in both model and prototype; then clearly

$$\frac{u_p(y)}{u_{rp}} = f\left(\frac{y}{xh_p}\right) \tag{3-5}$$

and

$$\frac{u_m(y)}{u_{rm}} = f\left(\frac{y}{xh_m}\right) \tag{3-6}$$

where x is a coefficient of proportionality, and the subscripts m and p refer to the model and the prototype respectively. It is noted that Eq. (3-5) and (3-6) can be reduced to Eq.(3-4) if we set $u_r = u_*$ and $xh = z_o$, or, since x must be the same constant for model and prototype:

$$\frac{z_{om}}{h_m} = \frac{z_{op}}{h_p} \tag{3-7}$$

Eq.(3-7) is in agreement with the conclusions drawn for the vertical scaling of the undisturbed boundary layer in a, i. e. if the ratio of the z_o values of model and prototype is set according to the desired vertical scale, then the ratio of the heights h must be chosen to yield the same vertical scale.

A choice of the value z_o and u_* fixes the boundary layer thickness at a given location in the wind tunnel, and thus the ratio h/δ_o. The assumption can then be made that the boundary layer thickness scales in the same ratio as the values z_o, or that

$$\frac{\delta_{om}}{\delta_{op}} \approx \frac{z_{om}}{z_{op}} \tag{3-8}$$

Of course, since z_o is, for rough boundaries, independent of velocities and location - at least for a uniform roughness cover, while δ_o depends both on velocity and on the fetch length, the assumption Eq. (3-8) is only a first approximation, which is probably more satisfactory for long fetch lengths than for short ones. An actual check of the validity of the assumption must come from a comparison of field and laboratory data.

d. The contribution of the drag integral term 4 of Eq. (3-1) must be the same for model and prototype. This condition is satisfied only if the distribution of c_f scales by using x/h as scaling parameter for the horizontal distance. Since it is well known (i. e. Schlichting, 13, p. 537) that c_f depends on the distance from the edge of the plate, that is, on the fetch length in the case of a natural boundary for smooth boundaries, the drag integral can only approximately scale according to Eq. (3-1). For rough boundaries, however, c_f is essentially a constant, and the drag integral becomes:

$$\frac{h}{\delta_o}\int_{x_a}^{x/h} c_f\,(x/h)\;\; d(x/h) \;=\; \frac{h}{\delta_o}\; c_f \int_{x_a/h}^{x/h} d(x/h) \;=\; \frac{c_f}{\delta_o}\;(x - x_a) \qquad (3\text{-}8)$$

Eq. (3-8) implies that the horizontal scale should be given by:

$$\frac{c_{fm}}{\delta_{om}} \cdot x_m \;=\; \frac{c_{fp}}{\delta_{op}} \cdot x_p \qquad (3\text{-}9)$$

or if $c_{fm} = c_{fp}$, that the horizontal scale is the same as the vertical scale, within the validity of the assumption on c_f.

e. The disturbed velocity profiles downstream from the obstruction must be similar for both model and prototype, with the same scaling parameters for the distributions as for the undisturbed velocity distribution. As far as modeling according to the momentum equation Eq. (3-1) is concerned, this is of course a sufficient condition, but not really a necessary one.

f. The momentum equation Eq. (3-1) must be valid. As will be shown in the next section, this is true only for distances downstream of x_a.

3.2 Validity of the Momentum Equation

The use of Eq. (3-1) is based on the validity of the boundary layer assumptions; - i. e. the assumption that gradients of quantities in the x direction (parallel to the boundary) are small compared with the gradients in the direction perpendicular to the boundary. Additional assumptions

are that the pressure distribution is determined only by the flow in the potential region outside of the boundary layer, so that the pressure is constant in the vertical. Also, gradients in the pressure along the direction of flow are neglected.

If the latter two assumptions are dropped, then the steady state boundary layer equations are given by

$$u \frac{\partial u}{\partial x} + v \frac{\partial u}{\partial y} = - \frac{\partial p}{\partial x} \frac{1}{\rho} + \gamma \frac{\partial^2 u}{\partial y^2}$$

with the equation of continuity

$$\frac{\partial u}{\partial x} + \frac{\partial v}{\partial y} = O$$

The system of equation is not complete without an additional equation for the pressure distribution. Customarily (Schlichting (13) p. 110), this equation is supplied by setting

$$u_a \frac{\partial u_a}{\partial x} = - \frac{1}{\rho} \frac{\partial p}{\partial x} = - \frac{1}{\rho} \frac{dp}{dx}$$

when u_a is the ambient velocity - i. e. the velocity in the potential core of the wind tunnel. The pressure gradient in the boundary layer flow is thus assumed to be independent of y, and the momentum equation (without consideration of any large surface forces like the drag of the hill) becomes:

$$\frac{\tau_o}{\rho} = \frac{d}{dx} \left(u_a^2 \theta \right) + \delta^* u_a \frac{du_a}{dx} \qquad (3\text{-}10)$$

as given by Karman (Schlichting (13) p. 139).

If the assumption that $\frac{\partial p}{\partial x}$ is independent of y is not made, then an additional term arises in Eq. (3-10) which is given to:

$$B = \int_0^{\delta} \left(\frac{1}{\rho} \frac{\partial p}{\partial x} + u_a \frac{du_a}{dx} \right) dy \qquad (3\text{-}11)$$

Thus the wall shear stress can be calculated from:

$$\frac{\tau_o}{\rho} = \underbrace{\frac{d}{dx}\left(u_a^2\,\theta\right)}_{\text{Term 1}} + \underbrace{\delta^*\, u_a \frac{du_a}{dx}}_{\text{Term 2}} \underbrace{- \int_0^{\infty} \left(\frac{1}{\rho} \frac{\partial p}{\partial x} + u_a \frac{du_a}{dx} \right) dy}_{\text{Term 3}} \qquad (3\text{-}12)$$

Eq. (3-12) can be used well to determine the validity of the assumptions on the pressure effect. If term 3 is small compared with term 1 and/or term 2, then the assumption that the pressure does not change across the boundary layer is justified. If term 2 is small compared with term 1, then the pressure gradient in the x direction is insignificant.

For checking the momentum balance expressed in Eq. 3-12, pressure measurements were made by using the static pressure holes of a pitot static tube and measuring vertical profiles of pressure. From these vertical profiles, horizontal pressure profiles were constructed for one model, the 2" x 2" wedge. The horizontal pressure profiles are shown in Fig. 10. Large pressure changes are found mainly at distances of up to 17h to 20h, where h is the model height. Further downstream, $\partial p/\partial x$ becomes approximately zero, but there still exists a marked difference between p values at different elevations y. This difference can be attributed to the high turbulent levels induced by the hill (which will be discussed further below), for it is well known that the equation of motion for turbulent flow in the direction perpendicular to the wall reduces, for boundary layer flows, to

$$-\rho \overline{v'^2} = p(y)$$

were $\overline{v'^2}$ is the average turbulent intensity in the y direction. (See Townsend (14)).

Experimental results obtained for the region downstream from the 2" x 2" wedge shaped hill model were used for checking Eq. (3-12).* The result of the calculations is shown in Fig. 11. The data are not sufficient to show the distance downstream of the hill at which the balance was obtained, but it is quite evident that up to a distance of 28" the contribution by term 3 is of significant magnitude and cannot be ignored. Its contribution is considerably larger than that of term 2 due to the change in pressure along the outer edge of the boundary layer, and it appears that both terms become negligibly small somewhere between 28" and 48" downstream from the model hill.

The resulting friction coefficient presents itself as the small difference between two large terms, i.e. term 1 + term 2 and term 3. The determination of term 3 which involves graphical construction of $\frac{\partial p}{\partial x}$ curves and their integration over the boundary layer is subjected to considerable error, since a small error in determination of the slopes causes a large error in the integral. The same is true for the slopes of the u_a^2 curve and the θ curve, so that the possible error is rather large. Thus, it is not surprising that the change from negative to positive friction coefficient takes place somewhat closer to the model than at the reattachment point, where it should occur theoretically. Also, the magnitudes of the friction factors are larger than one would expect.

Finally, it should be mentioned that the effect of the turbulence on the momentum balance has been neglected in Eq. (3-12). While this term is small, it might be sufficiently large to reduce the magnitude of the friction coefficient. The contribution by the turbulent quantities can be expressed by the term

$$\frac{d\theta_t}{dx} = \frac{d}{dx}\int_0^\delta \frac{\overline{u'^2}}{u_a^2}\, dy \qquad (3\text{-}13)$$

* The data are presented in dimensionless form by dividing each term by dynamic pressure of the outer flow $(1/2)\rho\, u_a^2$.

The slope can be given with some confidence only for two distances downstream from the hill model. The two points of

$$\frac{d}{dx} \int_0^{\infty} \frac{\overline{u'^2}}{u_a^2} \, dy$$

for 4" and 12" downstream from the model are shown in Fig. 11. They seem to contribute in the right direction.

3.3 Pressure Distributions

The most significant local effect of the model hill is found in its influence on the pressure distribution, both along the direction of the flow and perpendicular to it. The integral of the pressures in the direction of flow about the models yield the drag coefficient which is of significance in the determination of the momentum balance for the control volume enclosing the hill, as was shown in 3.1. The pressure along the floor might perhaps be used to yield an alternate way of determining the length L between the crest of the hill and the downstream reattachment point.

3.31 The Pressure Distributions Around the Models

The pressure around the models was measured with the help of pressure taps located at intervals of 1/8 h over the front and rear of the models. Typical results are shown in Fig. 12 and Fig. 13. From the measured pressure values, the drag per unit width was calculated by

$$D = \int_0^{h} (p - p_d) \, dy \qquad (3\text{-}15)$$

TABLE 2

Pressure profile parameters

Hill	L_o (ft)	U_a (fps)	p_{max} (mm Hg)	p_d (mm Hg)	$\frac{p_{max} - p_d}{1/2\rho u_a^2}$	C_D	C_o
1 x 4	13	15	0.035	0.034	0.89	0.839	0.95
	2	15	0.036	0.028	0.83	0.783	0.95
	25	15	0.027	0.033	0.77	0.755	0.98
	13	30	0.166	0.137	0.98	0.937	0.96
	2	30	0.146	0.120	0.86	0.845	0.98
	25	30	0.135	0.140	0.89	0.830	0.94
	13	45	0.34	0.31	0.93	0.892	0.96
	2	45	0.295	0.250	0.78	0.761	0.98
	25	45	0.28	0.30	0.83	0.810	0.98
	13	60	0.55	0.54	0.88	0.848	0.96
	2	60	0.48	0.41	0.71	0.692	0.98
	25	60	0.48	0.55	0.83	0.790	0.95
2 x 2	13	15	0.045	0.050	1.21	1.10	0.90
	13	15	0.047	0.035	1.025	0.997	0.97
	2	15	0.040	0.027	0.86	0.807	0.94
	25	15	0.044	0.023	0.86	0.808	0.94
	13	30	0.186	0.145	1.035	0.975	0.94
	2	30	0.155	0.117	0.88	0.813	0.93
	25	30	0.195	0.098	0.95	0.823	0.87
	13	45	0.44	0.29	1.025	0.978	0.96
	2	45	0.33	0.252	0.83	0.783	0.94
	25	45	0.43	0.21	0.92	0.820	0.89
	13	60	0.66	0.56	0.98	0.903	0.92
	2	60	0.55	0.41	0.768	0.717	0.933
	25	60	0.69	0.43	0.89	0.847	0.95

TABLE 2 cont'd

Hill	L_o (ft)	U_a (fps)	p_{max} (mm Hg)	p_d (mm Hg)	$\frac{p_{max} - p_d}{1/2\rho u_a^2}$	C_D	C_o
2 x 4	13	15	0.042	0.035	0.99	0.924	0.94
	13	15	0.036	0.035	0.92	0.863	0.94
	13	30	0.180	0.150	1.062	0.981	0.923
	13	30	0.180	0.130	1.00	0.962	0.96
	50	30	0.120	0.129	0.80	0.77	0.96
	13	45	0.38	0.29	0.96	0.893	0.93
	13	45	0.405	0.29	1.00	0.95	0.95
	13	60	0.66	0.62	1.03	0.916	0.91
	13	60	0.65	0.53	0.95	0.917	0.96
	50	60	0.44	0.45	0.72	0.675	0.94

where p is the pressure component in the direction of flow on the upstream face and p_d on the downstream side of the model. The drag coefficient is obtained from this equation by dividing by $1/2\ \rho\ u_a^2\ h$ where u_a is the ambient velocity at some significant reference point, and h the height of the model. All calculated parameters are listed in Table 2.

A difficulty arises in defining a suitable reference velocity. A small pressure drop occurs across the models, which is not compensated by a suitable expansion of the wind tunnel ceiling. The result is that the velocity in the test section core is slightly different upstream than downstream. The dynamic pressure due to the velocity at a distance of 3 ft upstream from the model in the potential cores was used for calculating the drag coefficients.

A parameter which is useful to check the consistency of the data is the factor C_o defined by the equation

$$C_o = \frac{C_D}{\frac{p_{max} - p_{dav}}{\frac{1}{2}\rho u_a^2}} \tag{3-16}$$

where p_{max} is the maximum pressure on the upstream side and p_{dav} is the average pressure over the downstream side of the model. As is easily recognized, the drag coefficient C_D is defined by the equation

$$C_D = \frac{p_{av} - p_{dav}}{\frac{1}{2}\rho u_a^2} \tag{3-17}$$

where p_{av} is the average pressure over the front of the model. Thus, C_o is a shape parameter which gives a measure of the deviation of the

actual pressure distribution over the whole model from a rectangular distribution with base $p_{av} - p_{dav}$ and height h. Since the distributions should not deviate very much for different velocities for a given model, C_o should change only slightly, and a large change in C_o would indicate likely errors in the experimental data. Such errors might well be due to an error in p_{max}, which has to be defined from smoothed readings.

The pressure profile parameters for the wedge shaped hill models are tabulated in Table 2. Data of pressure distributions were taken with the models both in the small sized tunnel and in the large sized tunnel. The distances between tunnel entrance and model location, denoted L_o, are covering a range from 2 to 50 ft, thus providing ample information on the effect of the boundary layer thickness on the pressure distributions or on the drag coefficients. However, no consistent pattern developed with either distance or velocity. This is in contrast to the findings of Plate (8) for a sharp edged fence, where the drag coefficient could be expressed for data taken over a similar range of distances and velocities by

$$C_D = 1.05 \left(\frac{h}{\delta_o} \right)^{2/7} \qquad (3\text{-}18)$$

Since it is unlikely that the drag coefficients for the wedge shaped hill depend on the boundary layer thickness in a much different way than those of the sharp edged fence, the scatter in the drag coefficients must be attributed to experimental error, or to peculiarities in the air flow pattern in the undisturbed boundary layer which had not been adequately evaluated before hand. A program is planned to check the drag coefficients again under better controlled conditions. This seems necessary in view of the importance which the drag coefficient has for the momentum balance.

Some of the inconsistencies of the data is revealed by inspecting the shape parameter C_o in Table 2, ranging in a rather random fashion all the way from 0.87 to 0.98. A more reliable set of data should improve

the results. It is expected that the coefficient C_o should not vary very much, but should be of the order of about 0.95 for all points, in agreement with the data on the fence.

Pressure distributions around the sinusoidal hill model have been measured for both the large wind tunnel and the small wind tunnel. The results have as yet not been evaluated.

3.32 Pressure Distributions Along the Floor

The pressure distributions along the floor were measured in order to find a way to define the downstream reattachment point, and to obtain an estimate on how far downstream the effect of the obstacle is felt in the flow. The third purpose was to find the pressure gradient which must be included in the calculation of the momentum balance downstream from the hill model.

Data were taken only for the wedge type models. The results are shown in Fig. 14, all for the small wind tunnel, since no data are available from the large wind tunnel. The data were plotted against x/h by first dividing the pressure difference between the local value and a reference pressure taken at a distance of 12 ft downstream from the model by the dynamic pressure in the center of the tunnel at the reference point. The results are rather striking.

First of all, it appears that the non-dimensional pressure distributions for wedge shaped hills of the same height are almost identical, and independent of velocity, everywhere except in the first region $x/h < 8$. The very steep pressure recovery from a non-dimensional pressure of -0.4 to approximately 0 takes place over a short distance of about 7h. The maximum pressure occurs at approximately 25h, while it is located for the 1" hill at about 30h. Significant differences are found, for the 2" hill models, only in the region $x/h < 7$. It appears

that the model with the longest slope leads to the lowest pressure directly downstream from the model. No conclusions can be drawn on the value of the absolute minimum, since both the 1 x 4 rear slope model and the 1 x 1 model have a lower minimum than the model with 1 x 2 rear slope.

An inspection of the curve for the 1" x 4" hill model in comparison to that for the 2" models show that the pressure recovery is approximately determined by the distance x/h from the model. However, the drop of the positive pressure downstream from x/h = 30 takes place more gradually, indicating that this region obeys a different law than can be expressed by nondimensionalizing x by h . It appears more likely, that the pressure drop is independent of model height i. e. a plot of the non-dimensional pressure coefficients vs x would yield parallel curves for different model heights.

3.4 The Velocity Distributions

In order to substantiate the general conclusions drawn above, a great number of mean velocity profiles has been taken. The data are presented, in tabular form, in Part 2 of this report. The velocity distributions are, however, summarized in Figs. 15 to 35. In the figures, four different types of information are given. At the top of each figure the ratio of the dynamic head Δh_a in the free stream at a given station to the dynamic head corresponding to the nominal velocity Δh_o is given. Below this curve, the profiles of mean velocity (solid dots) and of turbulent intensity (open circles) are shown. The scales for both distributions are usually given in the upper left corner of the figure. The fourth curve, below the velocity distributions, gives the pressure distribution along the floor obtained by dividing the difference Δh_p between the pressure at a given station and the pressure at the reference station by the dynamic pressure Δh_o corresponding to the nominal velocity.

The following presentations are based on only a partial analysis of the data. As a matter of routine, all parameters δ , δ^* , θ , and u_* were calculated. In these calculations δ was defined as that distance from the ground at which the velocity reached 0.995 of the value in the potential core. This is not an entirely useful definition in the zone where an appreciable vertical pressure gradient exists in the potential flow outside of the boundary layer, because in that region a constant velocity u_a is obtained only at a very large distance away from the wall. It seems more justified to define the boundary layer thickness in that zone as that thickness, at which the total head differs from the total head in the potential case by $0.005 : \frac{1}{2}\rho u_a^2$, where u_a is the nominal velocity head based on the velocity of reference taken some distance upstream from the model. One example of these calculations is shown in Fig. 36. It shows that at distances of 16" or 8h and further the boundary layer thickness defined in this manner is about the same as the distance of the velocity maximum from the ground in the velocity profile. Therefore, all calculations have been extended to the point of maximum velocity, which was used as a reference velocity.

With this reference velocity u_r (which differs from the velocity in the ambient air flow only for the small wind tunnel, and then only in the region extending to about 28" downstream from the model) the momentum thickness θ and the displacement thickness δ^* were calculated according to formulas:

$$\delta^* = \int_0^{\delta} \left(1 - \frac{u}{u_r}\right) \, dy \qquad (3\text{-}19)$$

and

$$\theta = \int_0^{\delta} \frac{u}{u_r} \left(1 - \frac{u}{u_r}\right) \qquad (3\text{-}20)$$

which were used for the further calculations. In particular, the so called profile shape parameter H is calculated which is defined as the ratio δ^*/θ . According to previous findings by Mueller et al. (5) this shape factor should be a function which depends on x/h and on the shape of the model only. As can be seen from Fig. 37, this is indeed the case for the sinusoidal hill. However, as shown in Fig. 38, the sharp edged wedges show marked differences with velocities in the large wind tunnel, but from a distance of about 30h downstream, the changes in H are only small, and a constant similarity curve is obtained for all hill models, regardless of size and rear slope. The differences between the curves for different velocities are probably due to the pressure gradients in the standing eddy region downstream from the hill.

3.41 Validity of Momentum Balance in Flow Direction

If Eq. 3-1 is valid for all data, then the location of the point x_3 , i.e. that point which marks the distance from the hill at which the positive contribution of the ground shear just cancels the negative contribution, should be found by simply calculating

$$\theta_o = \theta(x_3) - \frac{1}{2} C_D h \qquad (3\text{-}21)$$

From this equation the point x_3 can be found by plotting the right side of the equation against x and finding x_3 where θ_o = constant intersects the curve.

An example of this procedure is given in Fig. 39 for the large wind tunnel with the 2 x 4" wedge shaped hill. A value of x_3 is found at a distance of approximately 40 inches downstream from the hill. However, the 30 fps data in both the large and the small wind tunnel do not balance. It appears that the drag coefficient is too high, or the momentum thicknesses are too low. The latter is more likely, even though it is not clear why a systematic error should occur only in the 30 fps data.

3.42 The Shear Stress at the Wall

The shear stress at the wall plays a dual role in the determination of the velocity field downstream from the model hill. In the first place, the shear stress determines the velocity scale for the law of the wall, and thus it is the parameter which is required for the determination of the velocity distribution in the inner layer of the disturbed boundary layer. Secondly, the length scale of the velocity distribution should logically be described by the boundary layer thickness. The boundary layer thickness can be computed from Eq. (3-1), provided that the shear stress distribution at the wall is known.

No direct technique for measuring the shear stress was available. Indirect techniques can be used by assuming the validity of either the law of the wall, or some other empirical equation for determining the wall shear stress, or by using the momentum equation, Eq. (3-10) . The latter method is not very accurate due to the large effect of small errors in calculating the momentum thickness on the slope of the momentum thickness on the slope of the momentum thickness. The most commonly accepted shear stress equation is the equation of Ludwieg and Tillmann (3): (see also Schlichting (13) p. 575):

$$\frac{\tau_o}{\frac{1}{2}\rho u^2} = c_f = 0.246 \cdot 10^{-0.678H} \left(\frac{U_a \theta}{\nu}\right)^{-0.268} \qquad (3\text{-}22)$$

The friction coefficients calculated from this equation are listed in the summary tables (Part 2). As is immediately clear from the equation, numerical values can be computed if both H and θ are known in addition to u_a . In the present case, it seems that H could perhaps be assumed to be given by the plots Fig. 37 or 38. θ , however, can only be computed from Eq. (3-1) if the shear stress at the wall is known, i.e. if c_f is known. Thus, for a given H , C_D and δ_o of the flow

field, a calculation of θ would have to proceed by simultaneously solving Eq. (3-1) and Eq. (3-22) by trial and error. This procedure can become very tedious indeed, and it was therefore attempted to determine the shear stress by an empirical relation valid only for the particular hill model considered.

In carrying out this idea, it was first necessary to bring the asymptotic values of the shear stress distributions for different velocities into agreement. It is difficult to visualize that the zone where the shear stress is altered by the presence of the hill extends very far downstream. That is, there should exist, at some distance downstream from the hill, a point at which the shear stress is given by the stress that did exist before the model was installed. This value could then be found from considerations pertinent to the undisturbed boundary layer. The value of c_f corresponding to this point is denoted by c_{fo} and is the approximately asymptotic value which the actual shear stress reaches downstream from the hill. All data were thus made dimensionless by dividing them through c_{fo}.

A plot of c_f/c_{fo}, where c_f is the value of the local shear stress factor as calculated from Eq. (3-22), is shown in Fig. 40 for all cases of the 2" x 4" wedge. Considerable deviations about an average curve occur, but it requires direct shear stress measurements to find out whether the scatter of the data hides trends in Fig. 40 which are real.

3.5 The Flow Zones of the Disturbed Boundary Layer

The discussions of the previous articles show that the flow field consists essentially out of three different regions:

a. an undisturbed flow upstream from the model in which the boundary layer obeys the laws for the boundary layer along a smooth flat plate with zero pressure gradient,

b. a zone of highly disturbed flow in the neighborhood of the model, in which boundary layer assumptions are no longer valid,

c. a third zone, in which the boundary layer is gradually re-established, so that at some large distance downstream only the different boundary layer thickness will indicate the presence of a model.

The boundary between the three zones is not given by a vertical section through the boundary layer but rather by a curve $y = y(x)$, as is indicated in Fig. 41 which shows the flow regions. The undisturbed boundary layer does not, of course, end abruptly at the boundary, but there will be a zone in which the presence of the hill model profoundly, but gradually, changes the flow conditions, so that a transition layer exists between region 1 and region 2 of Fig. 41. It is logical that the change due to the hill is felt most strongly near the hill, and at a larger distance above the hill the effect might not be felt for some distance. Elliott (2) and Panofsky and Townsend (6) have discussed the case in which a discontinuity of the boundary configuration exists, and their researches led them to postulate a curve $y \propto x'^{m}$ where x' is the distance from the beginning of the discontinuity in surface configuration. Application of their reasoning to the present case, leads to a possible functional form for the boundary between regions 1 and 2 of.

$$y_1 = A_1 (x + x_1)^{m_1} \tag{3-23}$$

where x is the horizontal coordinate starting from the hill, A_1 is an (empirical) constant, depending on the geometry of hill and boundary layer, and x_1 is the distance of the origin of the boundary between zone 1 and 2 from the hill crest. This distance is difficult to define, but since the standing eddy region in front of the hill (which might or might not exist) is very short compared with the region of eddies downstream from the hill, one might put x_1 approximately equal to zero without much loss in accuracy. This is especially true since the origin and the first portion of the boundary falls into a region of large pressure changes, where the

simplifying assumptions of Elliott (2) or Townsend (15) cease to be valid.

The postulated curve separating zones 2 and 3 has also been shown in Fig. 41. It must start, perhaps not in a very well defined manner, at the point where the standing eddy zone ends, i. e. at the reattachment point of the separation stream line. This point is located at a distance L downstream from the hill crest. Consequently, a power law of the form postulated by Elliott, must for this case be of the form:

$$y_2 = A_2 (x - L)^{m_2} \qquad (3\text{-}24)$$

An appropriate functional form for this equation will depend on a knowledge of the distances L which were measured for this purpose.

3. 51 The Measurement of L

The distance L of the reattachment point from the model hill was measured by the dual wire technique described in 2. 23. A typical set of measurements used for the determination of L at 45 fps is shown in Fig. 42. The signal decreases quite rapidly with distance - at a rate of about 3 per cent per inch. The distance L is located where the curve with wire 1 facing the direction of flow intersects the curve with wire 1 downstream of wire 2. As a check, the procedure was repeated with wire 2; as can be seen from Fig. 42, small differences exist between the value from wire 1 and wire 2. The average between both values was taken.

Results of L measured in this manner as a function of velocity were plotted in Fig. 43. Up to a velocity of 45 fps the readings were quite repeatable, but beyond 45 fps, large differences were found at different times, and a significant drop in the length seems to be indicated. The reason for this strange behavior is not clear. A possible explanation might be given as follows.

Instantaneously, the standing eddy zone consists of a number of eddies trapped behind the model hill. These eddies are, however, not trapped completely; occasionally one of them moves too far toward the free stream line and is swept downstream by the flow. If such an eddy is not immediately replaced, there will occur changes in L of some duration, and perhaps at large velocities this duration can be of the order of the total sampling time. Systematic tests to check this hypothesis will be made in the near future.

Interesting as the changes of L with velocity are, they are not large enough to make much difference in the determination of the bounding curve between inner layer and intermediate layer of the boundary layer. Therefore, the distance L was assumed for all other cases to be about 12 times the height of the wedge shaped hills. An investigation of L for the sinusoidal hill has as yet not been undertaken. It will, however, be considerably shorter and might depend to a large extent on the ambient velocity.

3.52 The Criterion for Separation at Reattachment

The measurement of L with the accuracy afforded by the dual wire probe make it feasible to check the validity of applying criteria for separation to reattachment conditions. There exists some similarity between reattachment and separation. Both involve a stagnation point, but velocity profiles near separation in general will have a much smaller turbulence level than profiles at reattachment, and the validity of a separation criterion at reattachment is not at all assured.

A criterion for the beginning of separation has been given by Sandborn (11) in the form:

$$\frac{\delta^*}{\theta} = H = 1 + \frac{1}{1 - (\delta^*/\delta)} \qquad (3\text{-}25)$$

This criterion has been checked by Sandborn and Kline (12) against a number of available data and was found valid for all cases where the technique of measuring turbulent separation seem to suggest that actually the onset of separation, i. e. the region in which streaks of backflow are observed by visualization techniques, is measured rather than the point where the velocity is zero in the average. For fully separated laminar flow, a different relation is given by Sandborn (11) which is expressed by

$$\frac{\delta^*}{\delta} = \frac{2\sqrt{-\lambda}+1}{\left(\sqrt{-\lambda}+1\right)^2} \tag{3-26}$$

and

$$\frac{\theta}{\delta} = \frac{2\sqrt{-\lambda}+1}{\left(\sqrt{-\lambda}+1\right)^2} - \frac{2\left(\sqrt{-\lambda}\right)^2}{\left(2\sqrt{-\lambda}+1\right)^3} - \frac{2\sqrt{-\lambda}}{\left(2\sqrt{-\lambda}+1\right)^2} - \frac{1}{2\sqrt{-\lambda}+1} \tag{3-27}$$

where $\lambda = \frac{\delta^2}{\nu} \cdot \frac{du_a}{dx}$ is the so called Pohlhausen parameter (which is equal to -12 at separation for a velocity distribution approximated by a 4 term power series). The criteria were plotted according to Eqs. (3-25) to (3-27), ~~and~~ in Fig. 44, and are compared with actual experimental data based on distributions of mean velocities near the distance L measured with the dual wire probe. Data for both 45 fps and 30 fps are shown and conditions at L fall exactly on the curve for laminar separation, while only at about a distance of 26" is a point obtained which falls on the turbulent separation criterion.

Why the point corresponding to reattachment should fall on the criterion for laminar separation is not easily seen. Some arguments are advanced by Sandborn and Kline (12) to explain agreement of some turbulent separation data with the laminar separation curve, but these

arguments shall not be repeated here. It might be noteworthy that Plate (9) observed the reattachment for the case of a sharp edged fence with a streamer and found that velocity profiles taken at the reattachment points for the fences agreed well with the turbulent separation criterion instead of with the laminar one. The conclusion must be drawn that the definition of separation or reattachment depends to some extent on the method of determining reattachment. This conclusion is consistent with findings in supersonic flow by Roshko and Thomke (10) where different locations of the reattachment points were found for different techniques.

A calculated profile using a Pohlhausen parameter of -12 and the form of the velocity profile is given by Sandborn (11) for the laminar separation profile is shown in Fig. 45. The agreement of the experimental results with the calculated data is excellent.

3.53 The Boundaries Between the Flow Zones

The ideas expressed in the beginning of this section can now be checked qualitatively against experimental data obtained from the velocity distributions. As was mentioned previously, the ideas have not been verified for all data. The results can best be illustrated by using the data for the sinusoidal hill, however, one series of data which were taken for a wedge shaped hill are also included.

For obtaining the boundary layer regions it was found convenient to plot the velocity profile data on semi-logarithmic paper. In this presentation, region 2 will show as a very well defined straight line, and so does region 3. It does not present any difficulty to extend the lines for region 2 and region 3 until they intersect. The distance of this intersection from the floor is denoted with y_2 . An example of the technique of determining y_2 (and y_1) is shown in Fig. 36.

The definition of the boundary between region 1 and region 2 presents some difficulty since the transition between the two profiles is quite gradual.

The boundary was therefore obtained by plotting the undisturbed velocity profile over the measured disturbed profile. This was done by superimposing the plots of the two profiles on a light table until the two points $u/u_a = 0.995$ coincided. The boundary distance y_1 was found where the two profiles started to deviate from each other. The result of this procedure is not very accurate, and consequently the data exhibit considerable scatter.

The results for the inner boundary between region 2 and 3 are shown in Fig. 46. The length L for the 2 x 4" wedge hill was approximately known, and the length L for the sinusoidal hills was determined by trial and error, requiring that the best fitting curve through the data points be a straight line on double logarithmic paper. The slopes of these straight lines all are about 0.5, in other words, the equation for y_1 becomes

$$y_1 = A\,(x - L)^{0.5} \qquad (3\text{-}28)$$

The data are not sufficient to give a systematic account for the differences in the coefficient A . However, the exponent 0.5 is reasonably well established. This figure is quite different from the exponent 0.8 suggested by Elliott (2), perhaps because of the uniformly high turbulence level in the flow. As is well known, flows with high turbulence levels (like wakes and jets) behave like laminar flows in which the molecular viscosity γ is replaced by a constant eddy viscosity; consequently, it is perhaps possible to view the boundary layer development like the development of a laminar boundary layer, for which it can be shown (Schlichting (13) p. 241) that $\delta \propto \sqrt{x}$, as in the present case. The details of this analogy shall be worked out at a later date.

Fig. 47 shows the results attained for the outer boundary between region 1 and region 2. The results are quite unreliable, but a real boundary undoubtedly exists, especially since it cannot be found, for the 2 x 4" wedge at 60 fps, at distances larger than 72 inches. Whether the measured slope of approximately 0.3 is of any significance can at present not be determined.

3.54 The Shape of the Intermediate Profiles

The shape of the velocity profiles in the three regions of the boundary layer can be discussed only qualitatively, since not enough data, or theoretical knowledge, is available to estimate magnitudes over wide ranges of variables.

A typical example of profiles plotted on logarithmic paper is reproduced in Fig. 48. The redeveloping boundary layer at the floor in zone 3 and the boundary layer in zone 2 are well defined straight lines. The profile in zone 3 should obey the law of the wall, i.e. the velocity distribution should be described by a law of the form

$$\frac{u}{u_*} = \frac{1}{k} \ln y + B \qquad (3\text{-}29)$$

where B is a term depending essentially only on the roughness of the boundary and (perhaps) on the pressure gradient. A detailed investigation of this layer will be made in the near future.

Of great significance is the fact that in all profiles the portion corresponding to zone 2 is found to yield a well defined straight line slope with a slope which appears to be independent of x . Thus, the velocity distribution can be expressed by

$$\frac{u}{u_a} = A \ln y + C \qquad (3\text{-}30)$$

where A is constant for a given ambient velocity and hill model. A number of different values of A are given in Table 3. Systematic changes of these values with velocity and with model type must be expected; but the data do not permit to establish definite relationships. However, it is known (Plate (8)) that for a model consisting of a sharp edged fence the coefficient A can be expressed by

$$A = 1.3 \, (h/\delta_o)^{2.5} \qquad (3\text{-}31)$$

TABLE 3

Coefficient A for different models

Hill	u_a	Slope A	δ
2 x 4	30 fps	0.57	13"
2 x 4	60 fps	0.57	13.5"
4 x 20	30 fps	0.42	13"
4 x 20	60 fps	0.46	13"
2 x 10	30 fps	0.415	14"

where h is the fence height and δ_o is the boundary layer thickness at the location of the model for the undisturbed boundary layer. Investigations to systematically determine the dependency of A will be undertaken in a continuing effort to provide a basis for calculating the velocity distributions in the zone downstream from a two dimensional roughness.

3.6 Turbulence Data

A fair idea of the pattern of turbulence generated by hill model and by the wall can be obtained by studying the turbulent component in the direction of flow $\overline{u'^2}$, or the turbulent intensity $\sqrt{\overline{u'^2}}/u$, where u is the mean velocity corresponding to the point at which $\overline{u'^2}$ has been measured. Arie and Rouse (1) have shown that in the region around the separation streamline distributions of $\overline{u'^2}$, $\overline{v'^2}$ and $\overline{u'v'}$ are roughly similar so that a qualitative picture of the turbulence generated by the hill models can be obtained from an inspection of the distribution of the turbulent component in the flow direction which can be measured much more readily than the other two turbulent quantities. It was also shown empirically by Plate (9) that a quantity based on the component $\overline{u'^2}$, namely the contribution θ_t of $\overline{u'^2}$ to the momentum equation given by

$$\theta_t = \int_o^{\delta} \frac{\overline{u'^2}}{u_a^2}\, dy \qquad (3\text{-}32)$$

can be used quite well to scale the spreading parameter of a plume of a diffusing gas in the boundary layer disturbed by a sharp edged fence, and a similar behavior can be expected also for the case of the hill models.

The profiles of $\overline{u'^2}$ are shown in the Figs. 15 to 35. Qualitatively, the profiles have, for some distance downstream from the hill, an appearance which is remarkably similar to that of a two-dimensional jet. This similarity extends as far as showing essentially a linear spread of the intensity profiles for a distance as far downstream as 60h, where h is the model height. This fact is documented in Fig. 49 for a 2" x 4" wedge

in the 60th wind tunnels. The "intensity jet" width σ_t was defined as that distance from the floor at which the value of $\overline{u'^2}$ had dropped to half the maximum value. No corrections were made for defining the origin of this jet. As Fig. 49 shows, the origin certainly does not coincide with the location of crest of the hill, but a virtual origin exists at some distance above or upstream from the crest of the hill. This is in agreement, at least qualitatively, with the results obtained for a two-dimensional jet. The analogy between the "intensity jet" and the two-dimensional jet should however not be taken too literally. In reality, the large turbulence levels are due to the steep gradient in the velocity profile near the separation streamline, and the amount of turbulence present is determined by the balance of generation and dissipation of turbulent energy, and not by the law of preservation of momentum which appears to govern the equations for the mean velocity distributions in a jet (Schlichting (13) p. 593).

A convenient measure of the integral characteristics of the turbulence field - i. e. a measure which describes the average of the turbulence across the disturbed boundary layer - is found in θ_t as determined by Eq. 3-32. Examples of the variation of θ_t with distance are given in Fig. 50, for the 2" x 4" wedge. The figure demonstrates well the very steep increase in turbulence near the hill, and the fairly rapid decay of the average turbulent energy with distance. A quantitative evaluation of these results is, however, at present not possible, and shall be attempted in connection with the evaluation of data for turbulent diffusion in the flow from a model hill.

Locally, the turbulence is best analyzed by means of intensity spectra. The spectra were obtained for a sinusoidal hill model of 2" height in the small wind tunnel at a velocity of 30 fps. Four different positions were chosen, one directly above the crest of the hill, with a hot wire located as closely to the crest as possible, the second position

was as the first, except the wire was at a distance of 1/4" above the crest. The data reproduced in Fig. 51 show that there is no large difference in the profile shape - indicating the fact that no new turbulence is generated which might shape the spectrum at high frequencies. Significant is, however, the well defined maximum at approximately twelve cycles per second. This peak might be indicative of the large scale eddies that are probably being shed by the hill. The peak is more clearly defined in the data taken very close to the hill crest.

In Fig. 52, the data taken very close to the crest are compared with data taken further downstream, 9" and at 1' - 9" downstream from the crest, at a distance of about one inch from the floor. The difference is remarkable. The maximum is much less pronounced, the energy at low frequencies has increased - signifying the increase in turbulent energy extracted from the mean flow by the large (or low frequency) eddies. On the other hand, the profile at higher frequencies drops off quite linearly in the double logarithmic presentation. The best fitting straight line has a slope which is almost precisely - 5/3. Thus, the conclusion can be drawn that the spectrum is in inertial equilibrium over a wide region. This, on the other hand, is found also for spectra taken in the atmosphere, so that one may conclude that the turbulence spectra downstream from an obstruction in the wind tunnel resembles that of the atmospheric boundary layer much closer than those in ordinary boundary layer flow in a wind tunnel. A possible significance of this result is that it can be expected that atmospheric diffusion models based on the -5/3 power law for the spectrum should work also in the wind tunnel downstream from 2 dimensional obstructions. This finding should greatly increase the probability of obtaining suitable model laws for modeling a diffusion pattern in a wind tunnel.

4. OUTLINE OF CONTINUATION OF WORK

The investigation which was reported on was concerned with two problems. The first problem was that of modeling the flow downstream from a two-dimensional hill in a wind tunnel. It is shown that this is entirely feasible since the momentum equation and the velocity distributions are described by the same set of parameters. Since the modeling ignored essentially the turbulence characteristics, except in as far as they are reflected in the mean flow parameters, it is not clear how diffusion processes would model. It is this aspect of the problem which will be covered most extensively in the continuation of the program.

The second problem concerned the prediction of velocity distributions downstream from a two-dimensional hill on the basis of knowledge of the hill geometry and of the undisturbed boundary layer. Only some initial investigations were made towards solving this problem, from which it appears that two problems are to be solved in succession. First, an effort has to be made to predict the potential flow region about the model hill with the purpose of obtaining pressure distributions at the vertical section through reattachment, and the boundary layer thickness and displacement thickness at reattachment. The information on displacement thickness and boundary layer thickness can be used to calculate the profile of velocities at reattachment by first determining the Pohlhausen parameter at reattachment through use of Sandborn's separation criterion and then calculating the corresponding velocity profile. This phase of the program is under investigation, but no conclusions can be given, except that a simple representation of the flow in the potential zone outside the boundary layer above the hill model by means of the flow about an equivalent circular cylinder did not yield satisfactory results even at the crest of the hill.

The second part of the problem consists of the prediction of the flow field downstream from reattachment once the pressure and the velocity distribution at reattachment are known. The most promising approach seems to be to use a modified version of the model of Elliott (2) by starting a boundary layer development consistent with the law of the wall at reattachment and by using the profile at reattachment as the outer profile. Junction conditions are found by assuming Bernoulli's equation to hold along any streamline which crosses from the outer flow into the inner flow, and by making a suitable assumption on either the continuity of the shear stress (as was done by Panofsky and Townsend (6)) or the continuity of the velocity profile (as was done by Elliott (2)).

Concurrent with these analytical investigations will go an experimental program on the diffusion characteristics of the flow field downstream from the model hill.

5. BIBLIOGRAPHY

1. Arie, M. and H. Rouse: "Experiments on two-dimensional flow over a normal wall." Journal of Fluid Mech., Vol. 1, 1956.

2. Elliott, W. P.: "The growth of the atmospheric internal boundary layer." Transactions AGU, Vol. 39, No. 6, 1958.

3. Ludwieg, H. and W. Tillmann: "Investigation of the wall shearing stress in turbulent boundary layers." NACA, TM 1285, 1950.

4. Man Moon, I.: "Direction sensitive hot wire anemometer for two-dimensional flow study near a wall." ASME Symposium on Measurement in Unsteady Flow, Worchester, 1962.

5. Mueller, T. J., H. H. Korst and W. L. Chow: "On the separation, reattachment and redevelopment of incompressible turbulent shear flow." Transactions ASME, Journal of Basic Engineering, Paper No. 63 - AHGT-5, 1963.

6. Panofsky, H. A. and A. A. Townsend: "Change of terrain roughness and the wind profile." Quarterly Journal Royal Met. Society, Vol. 90, 1964.

7. Plate, E. J. and J. E. Cermak: "Micrometeorological wind tunnel facility." Final Report on Contract No. DA-36-039-SC-80371, U. S. Army, CER63EJP-JEC9, Colorado State University, Fort Collins, Colorado, 1963.

8. Plate, E. J.: "The drag on a smooth flat plate with a fence immersed in its turbulent boundary layer." ASME paper no. 64FE17, presented at the Fluid Engineering Conference, May 18-21, 1964, Philadelphia, Pennsylvania.

9. Plate, E. J.: "Ein Beitrag zur Berechnung von Austauschvorgängen in der durch eine undurchlässige Hecke gestörten bodennahen Luftschicht." Dissertation submitted to Technische Hochschule Stuttgart, Germany, 1964.

10. Roshko, A. and G. J. Thomke: "Flow separation and reattachment behind a downstream - facing step." Report SM-43056-1, Douglas Aircraft Company, Missile and Space Systems Division, Santa Monica, California, 1964.

Bibliography cont'd

11. Sandborn, V. A.: "An equation for the mean velocity distribution of boundary layers." NASA Memorandum, 2-5-59E, 1959.

12. Sandborn, V. A. and S. J. Kline: "Flow models in boundary layer stall inception." ASME, Journal Basic Engineering, Paper No. 60WA149, 1960.

13. Schlichting, H.: "Boundary layer theory." 4th ed. McGraw Hill, 1962.

14. Townsend, A. A.: "The structure of turbulent shear flow." Cambridge University Press, 1957.

15. Townsend, A. A.: "The behavior of a turbulent boundary layer near separation." Journal of Fluid Mechanics, Vol. 12, 1961.

APPENDIX A : Figures

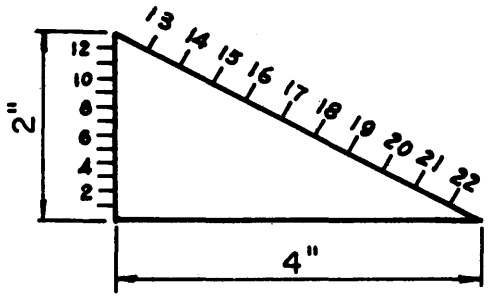

Wedge 2" x 4"

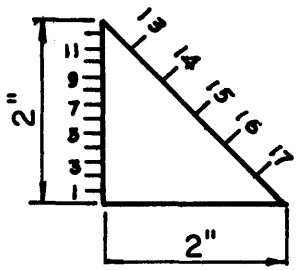

Wedge 2"x 2"

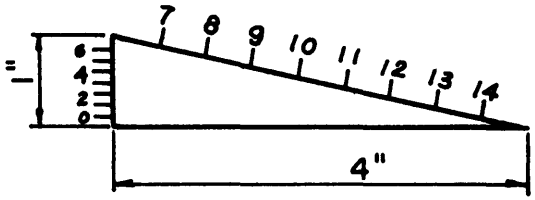

Wedge 1" x 4"

NOTE: The pressure taps are indicated by numbers. They are 1/8" apart in vertical distance, except sinusoidal hill 20" x 4" where they are 1/4" apart and wedge 1"x 4" where the distance is 1/16".

L	H
10"	2"
20"	4"

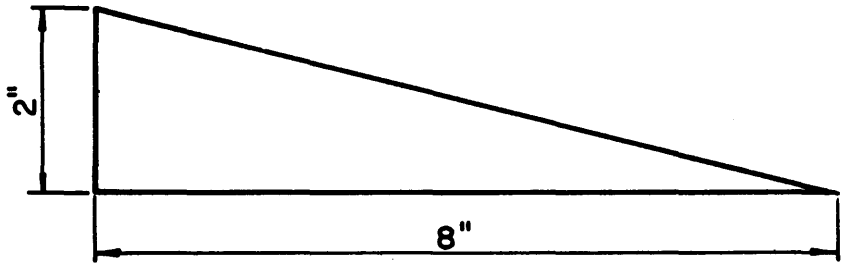

Wedge 2" x 8"

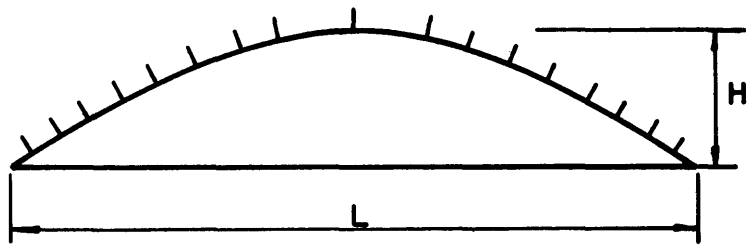

Sinusoidal hill

FIG. 1 MODELS OF HILLS

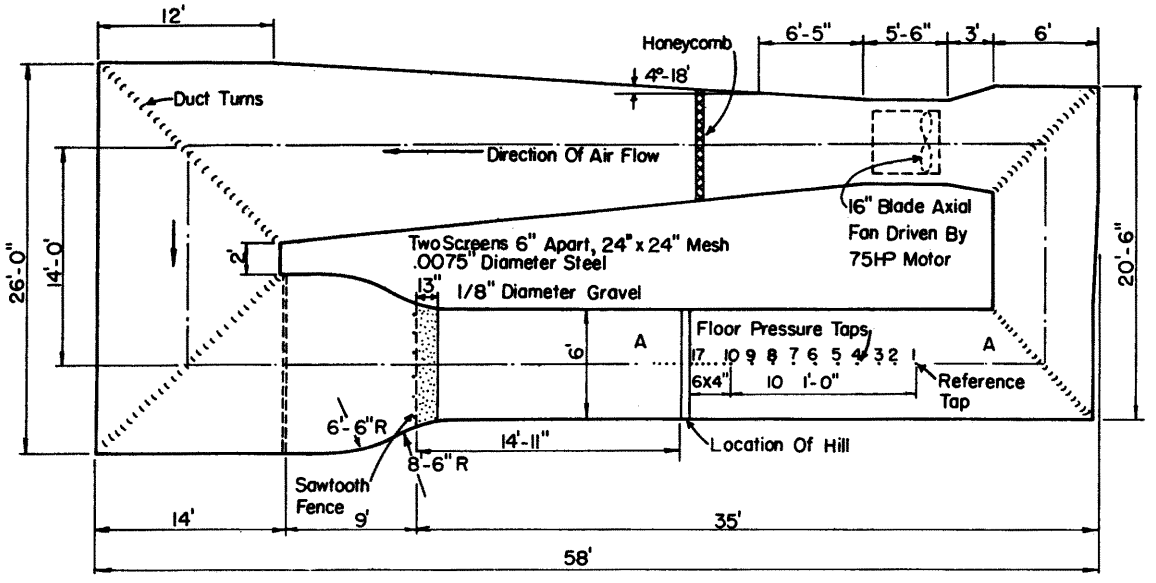

PLAN VIEW

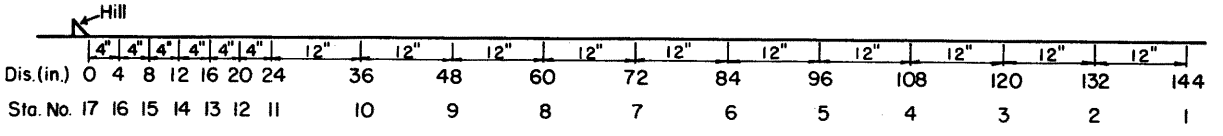

SECTION A-A

FIG. 2 SMALL WIND TUNNEL

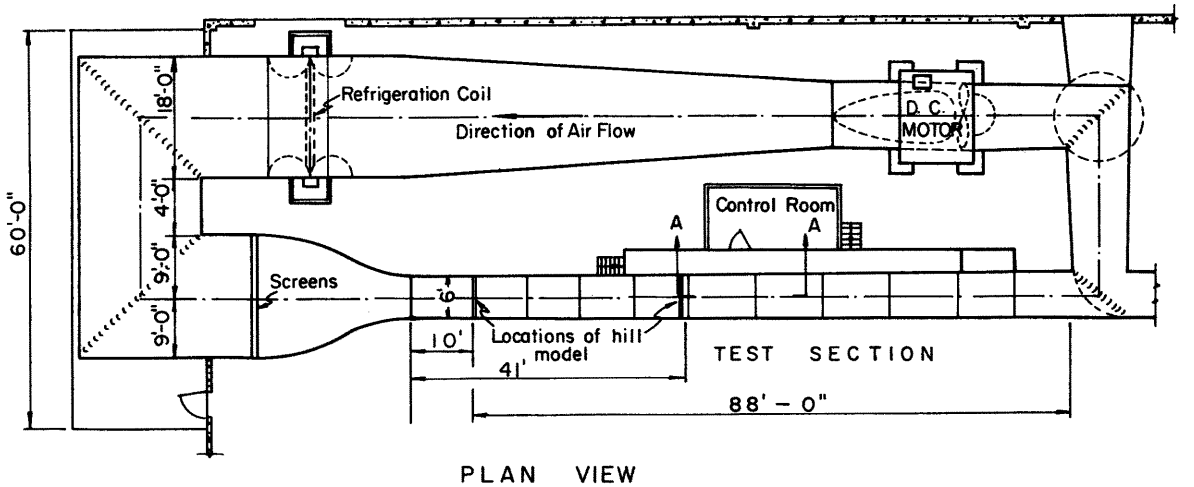

PLAN VIEW

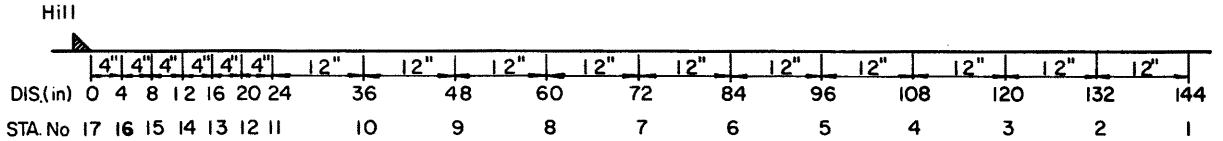

SECTION A-A

FIG. 3 LARGE WIND TUNNEL

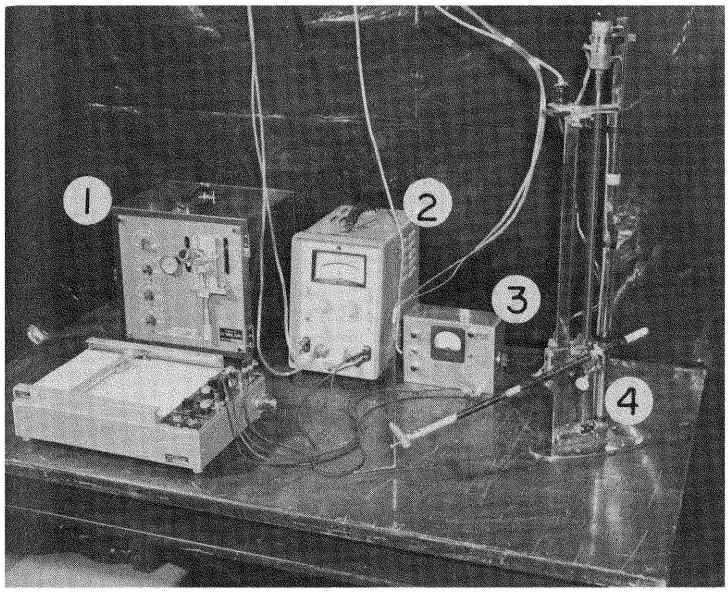

1 micromanometer
2 electronic micromanometer
3 positioner control
4 probe positioner with pitot-static tube

Fig. 4. Pressure measuring equipment.

1 magnetic tape recorder
2 true rms meter
3 hot-wire amplifier
4 probe positioner with hot-wire probe

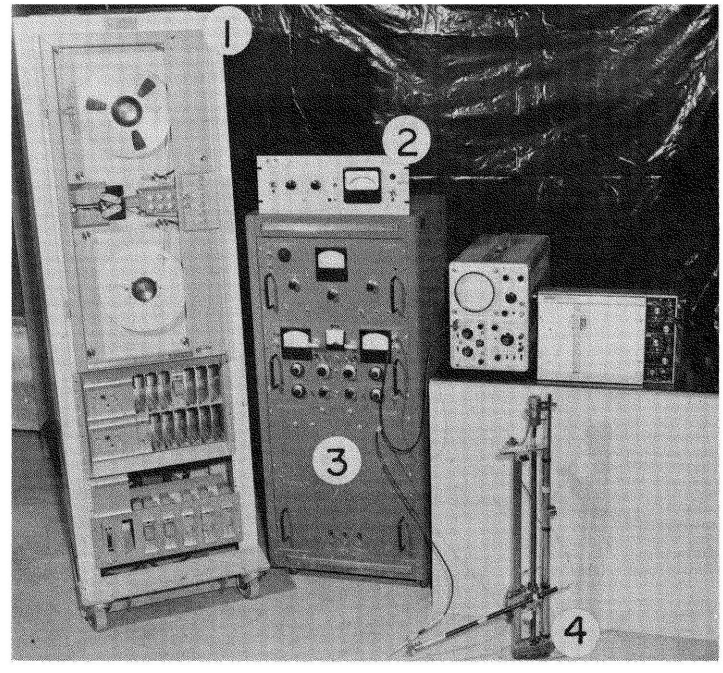

Fig. 5. Turbulence measuring equipment.

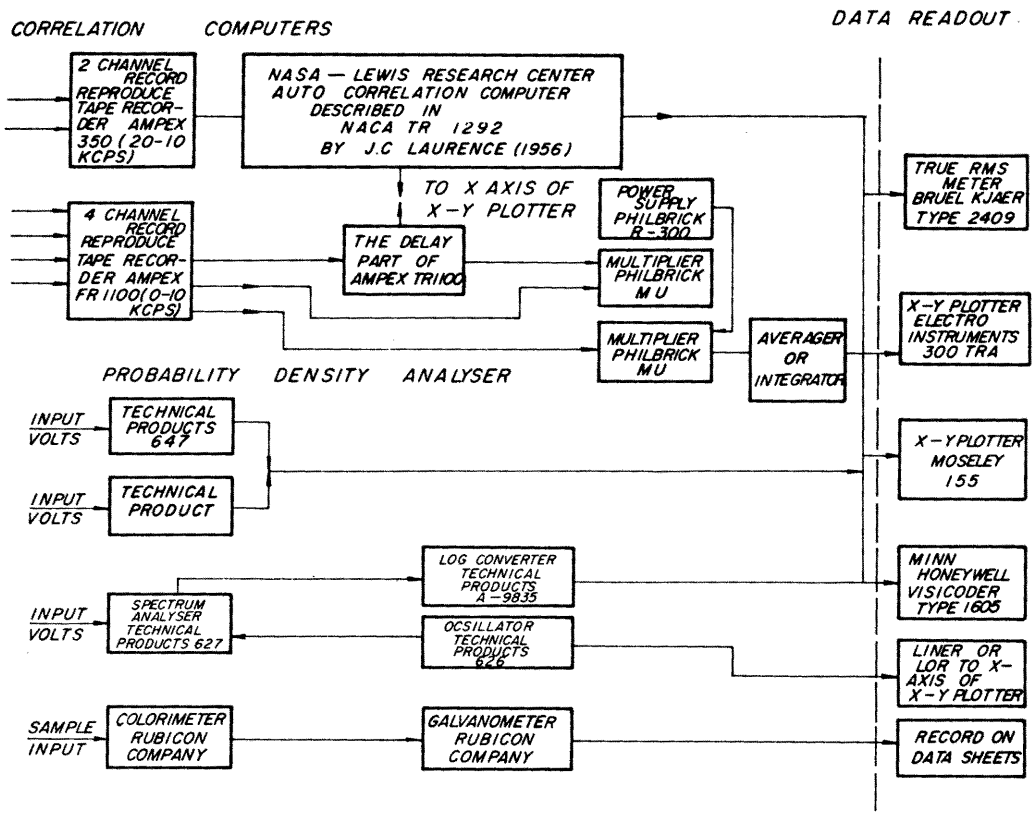

FIG. 6 SCHEMATICS OF THE ANALOG COMPUTING EQUIPMENT

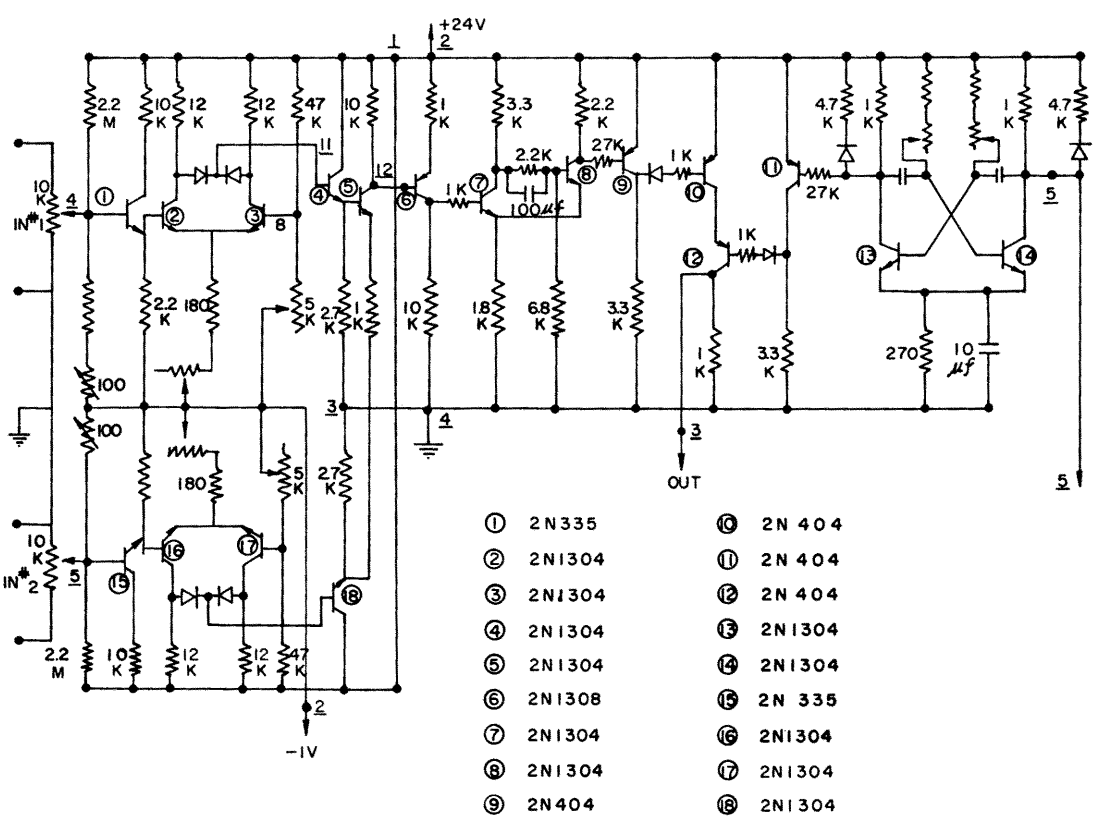

FIG. 7 DISCRIMINATOR CIRCUIT

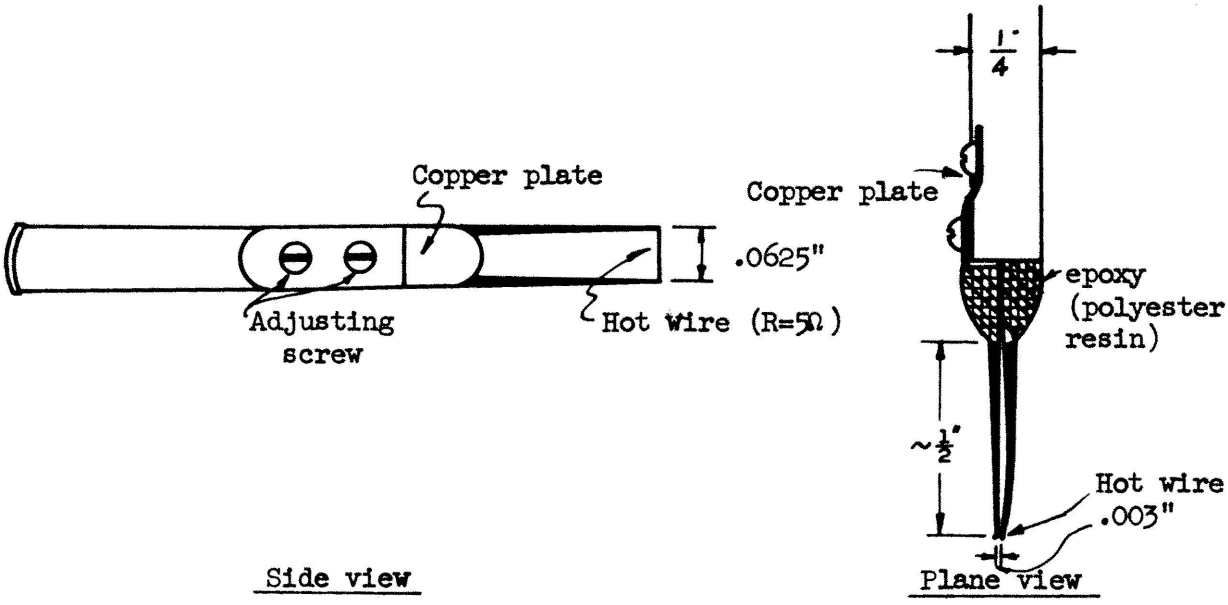

Fig. 8. Two wire probe of reattachment measuring equipment.

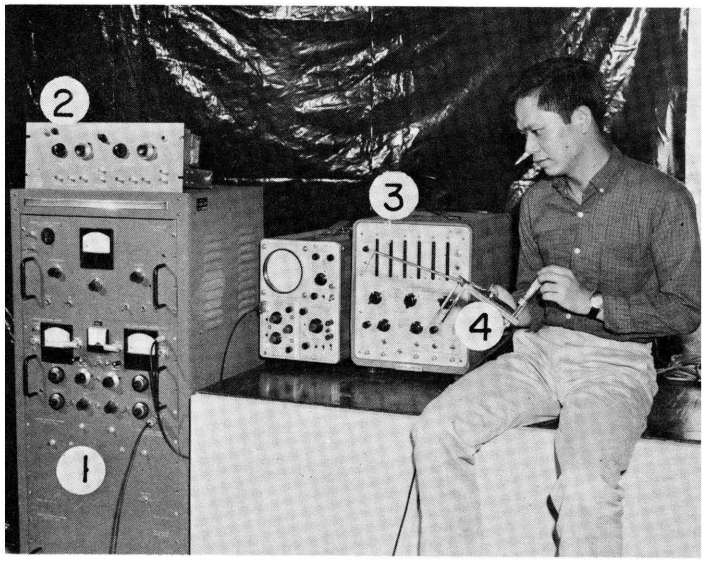

1 hot-wire anemometer amplifier

2 discriminator circuit

3 frequency counter

4 dual wire probe

Fig. 9. Equipment used in measuring the reattachment point.

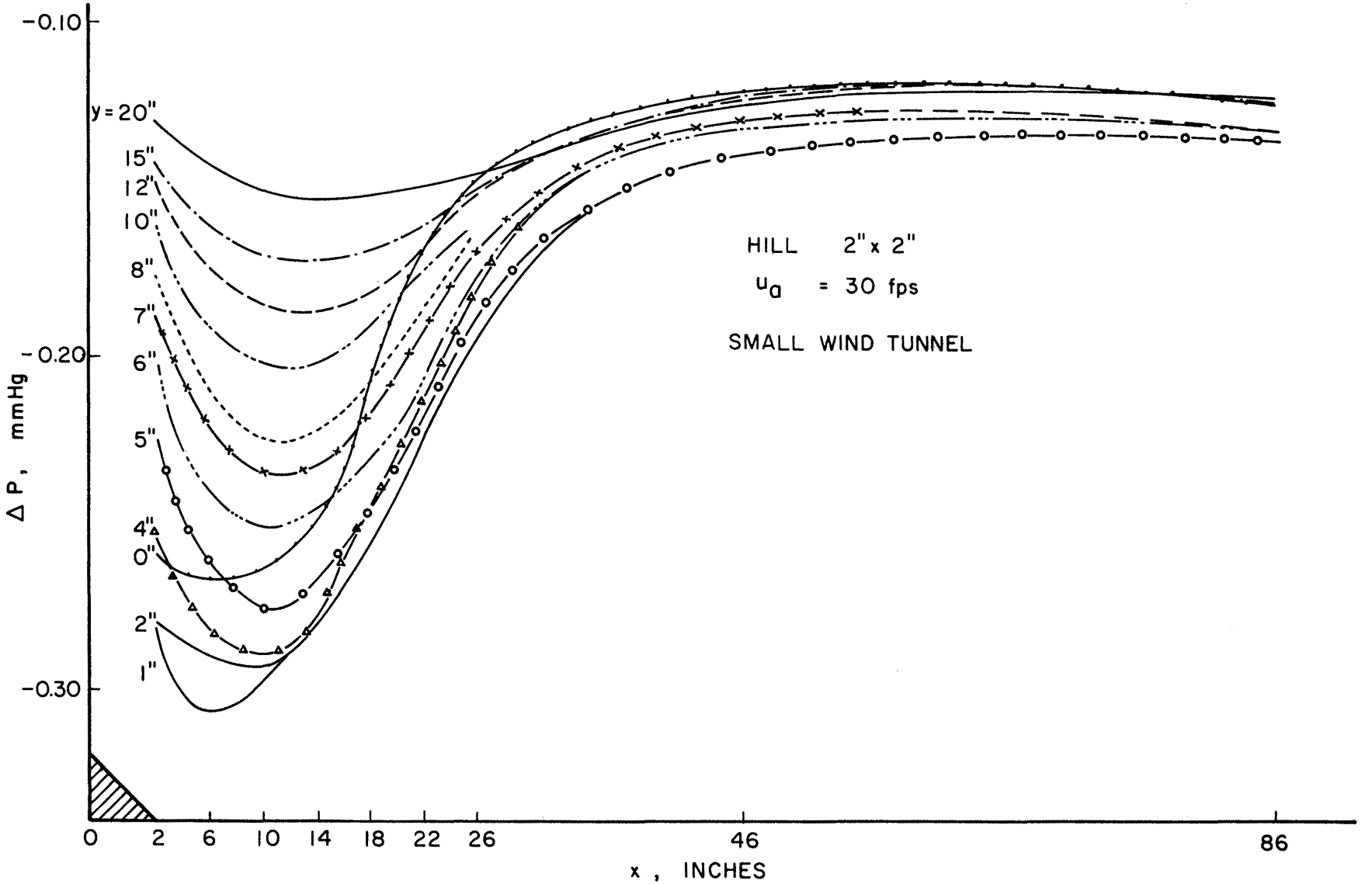

FIG. 10 HORIZONTAL PRESSURE DISTRIBUTION

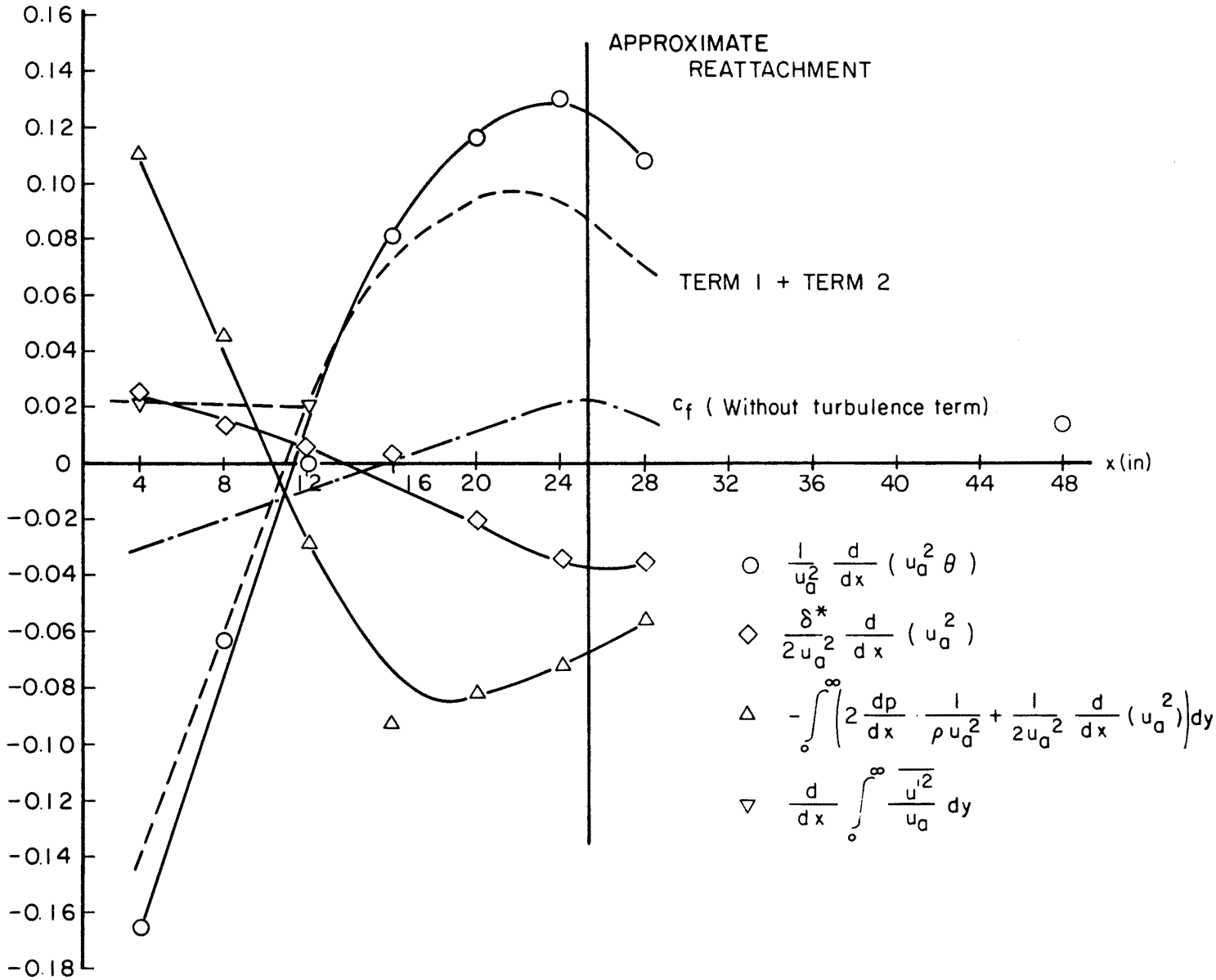

FIG. 11 MOMENTUM BALANCE DOWNSTREAM FROM THE MODEL HILL

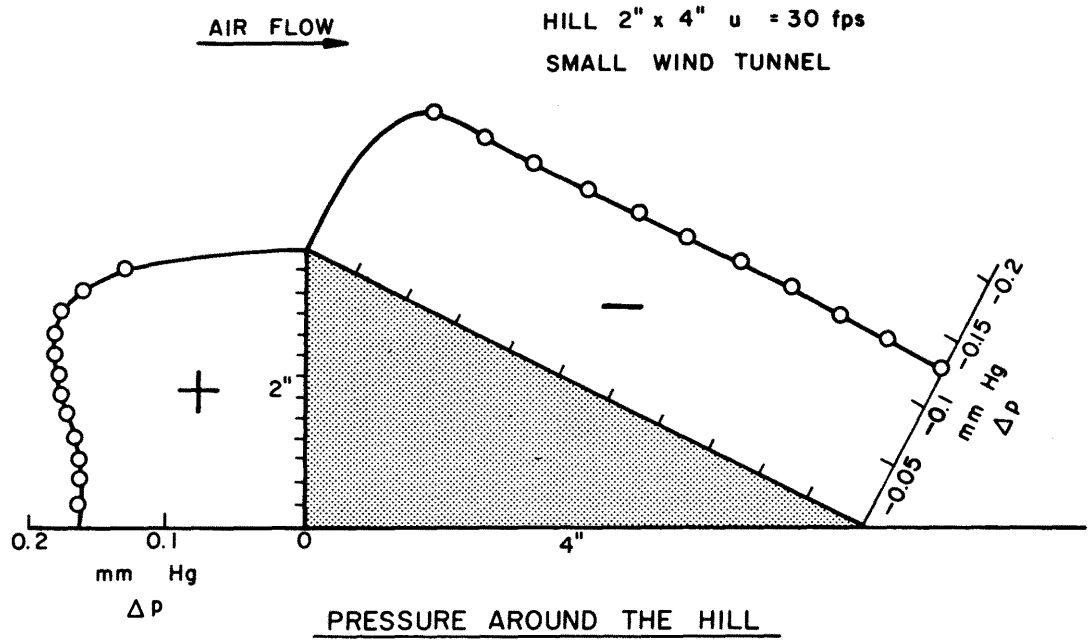

FIG. 12 TYPICAL PRESSURE DISTRIBUTION ABOUT WEDGE SHAPED HILL

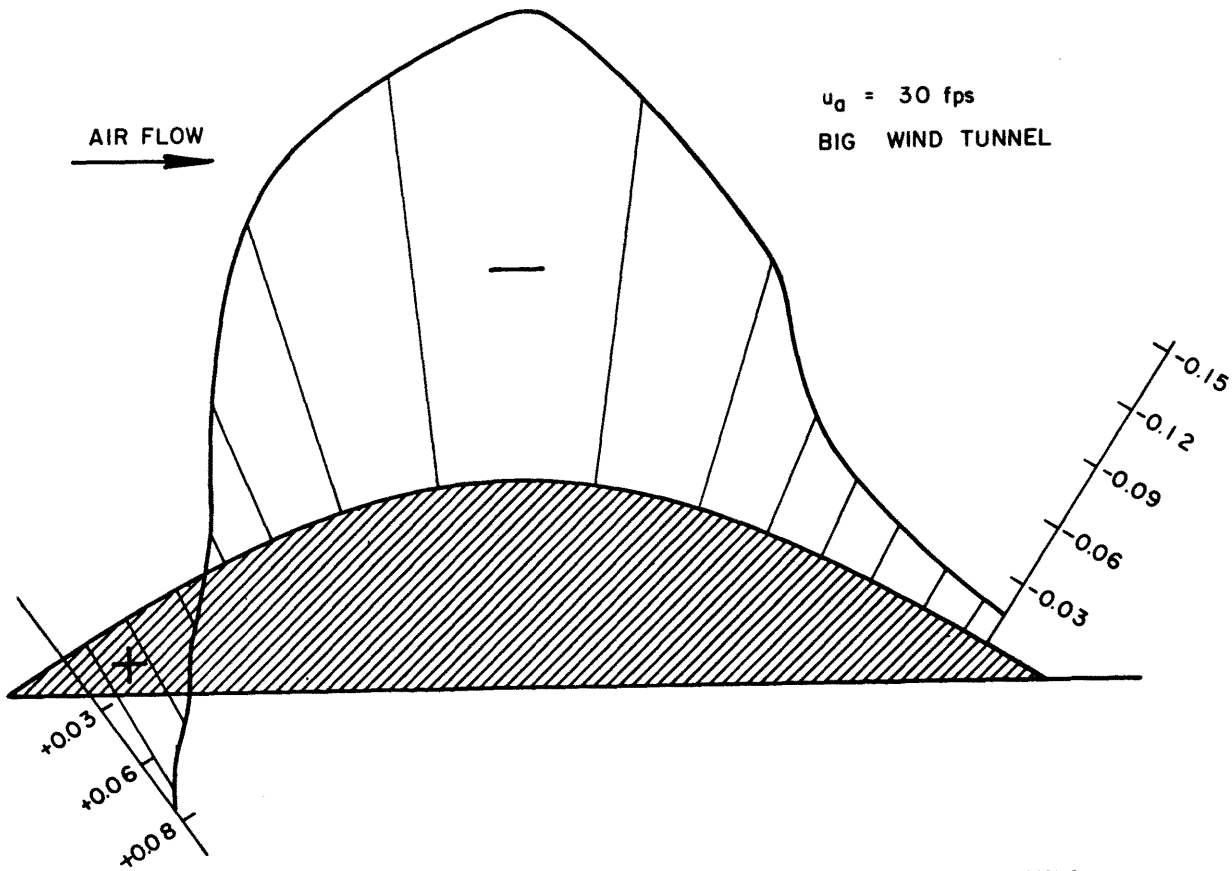

FIG. 13 TYPICAL PRESSURE DISTRIBUTION ABOUT SINUSOIDAL HILL

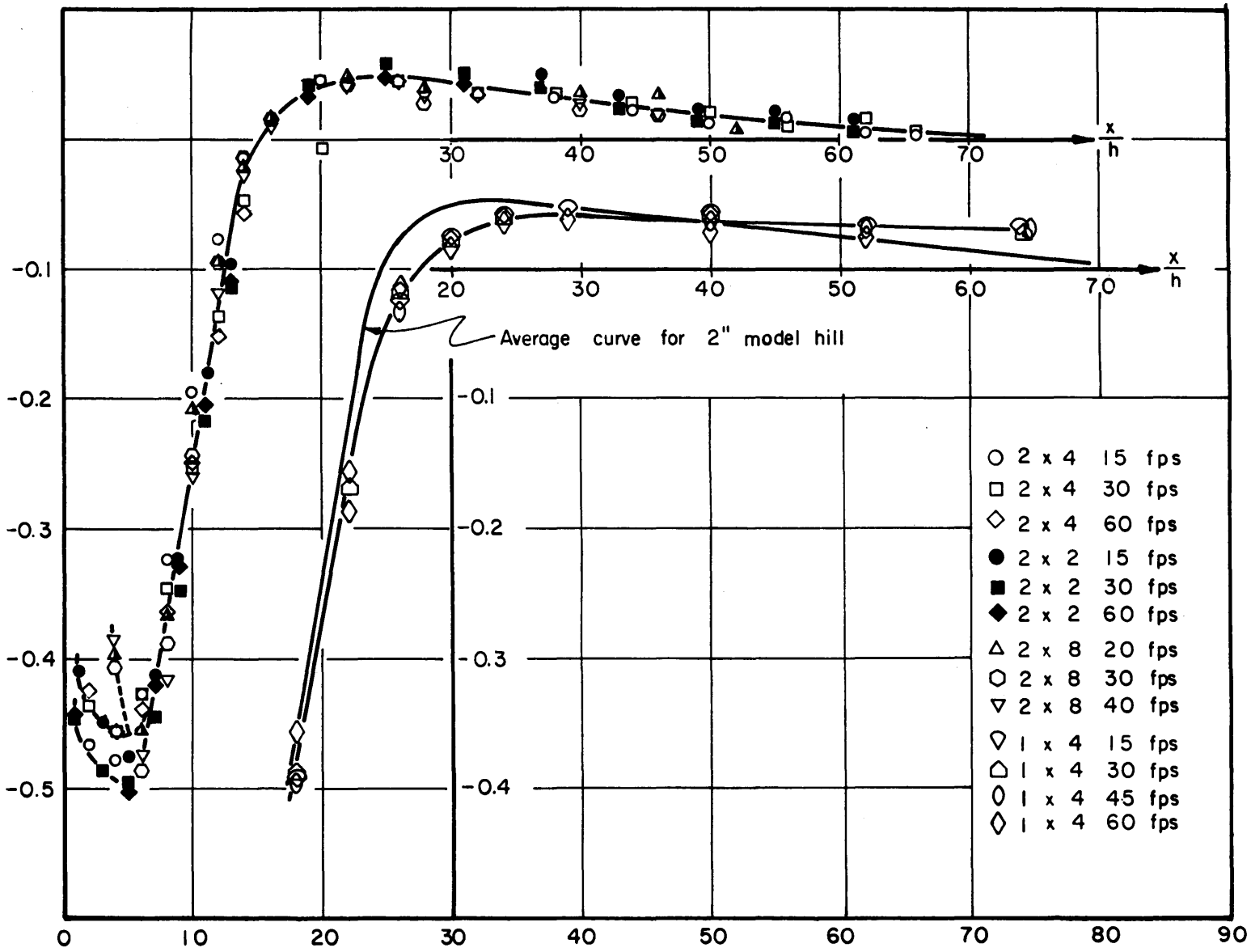

FIG. 14 PRESSURE DISTRIBUTIONS ALONG WIND TUNNEL FLOOR

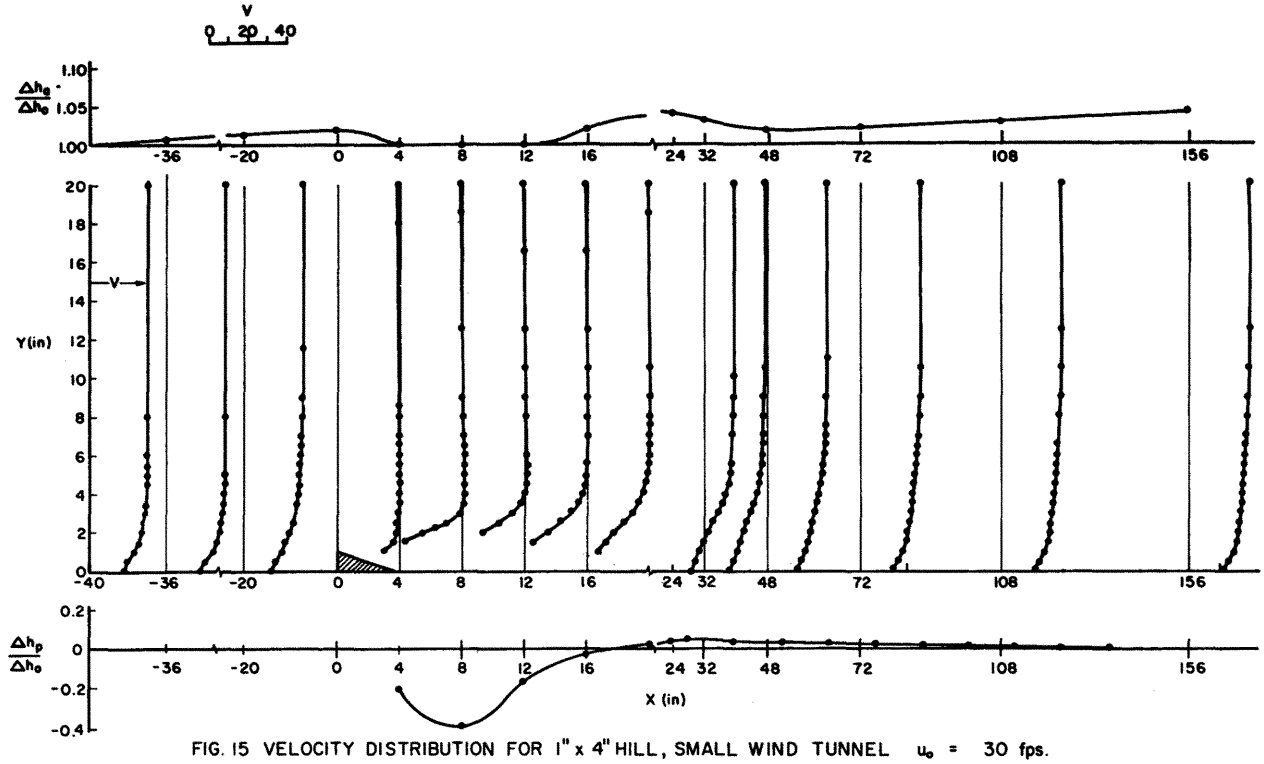

FIG. 15 VELOCITY DISTRIBUTION FOR 1" x 4" HILL, SMALL WIND TUNNEL u_o = 30 fps.

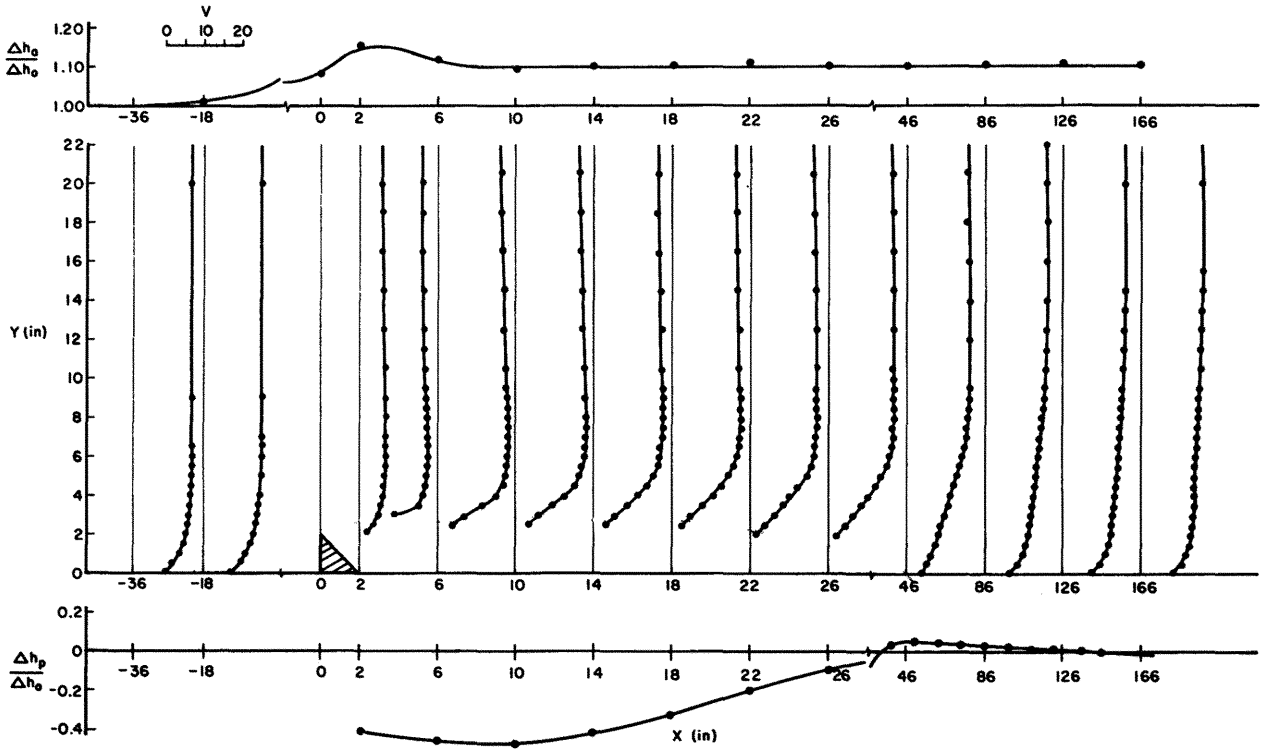

FIG.16 VELOCITY DISTRIBUTION FOR 2"x 2" HILL, SMALL WIND TUNNEL $u_0 \sim 15$ fps.

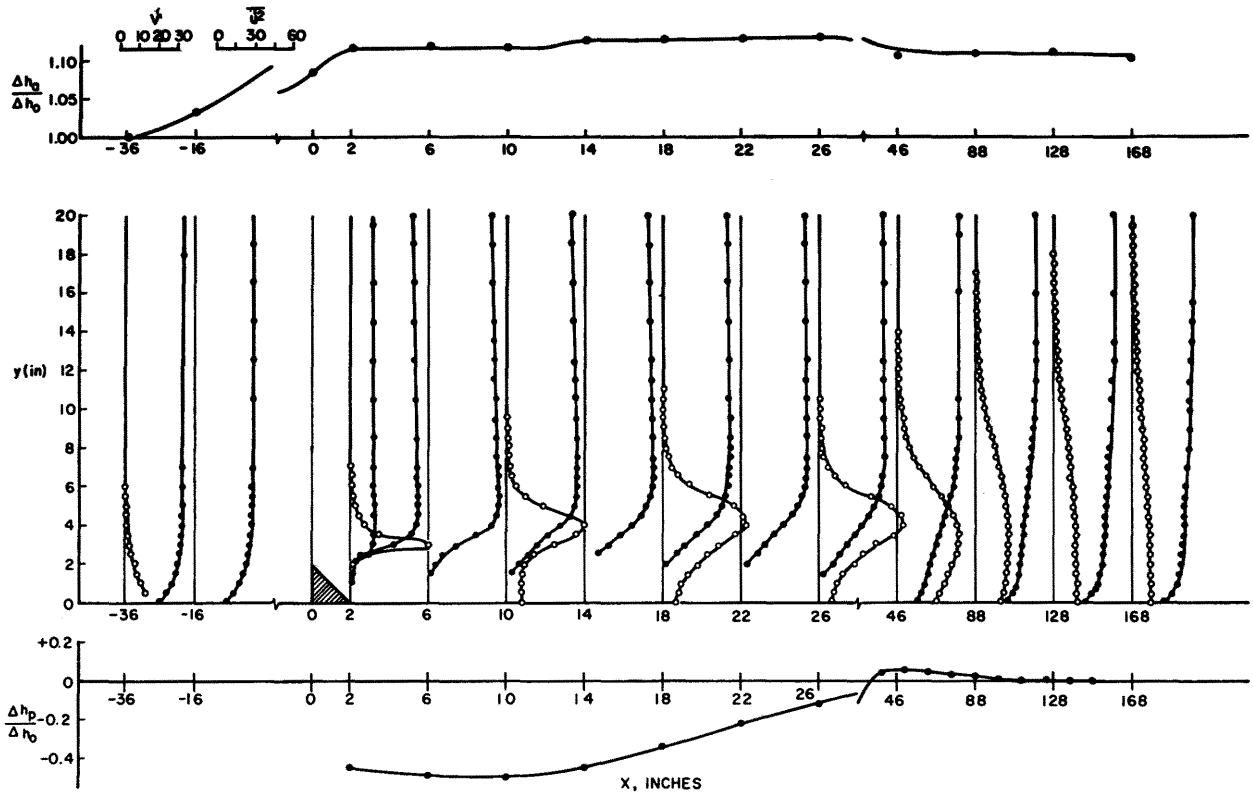

FIG. 17 VELOCITY DISTRIBUTION FOR 2" x 2" HILL, SMALL WIND TUNNEL u_0~30 fps

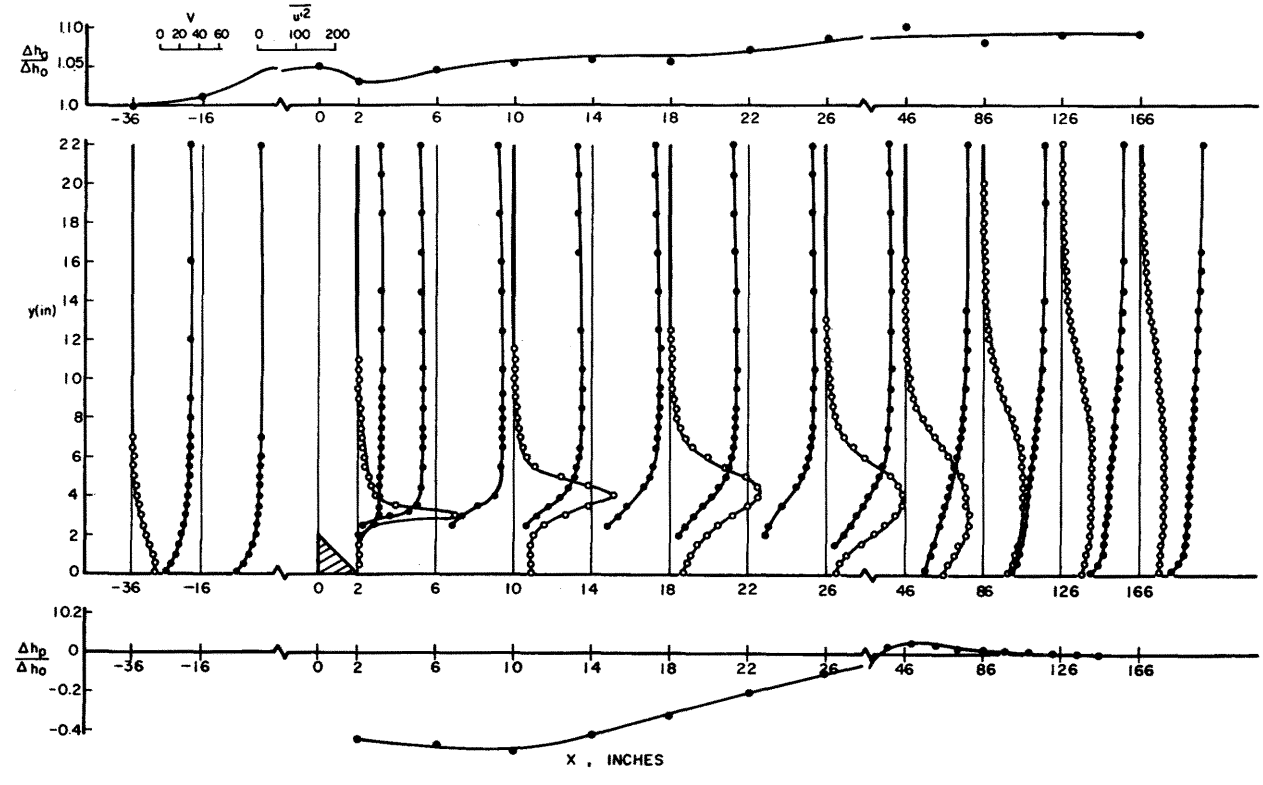

FIG. 18 VELOCITY DISTRIBUTION FOR 2"x 2" HILL, SMALL WIND TUNNEL u_0 ~ 60 fps.

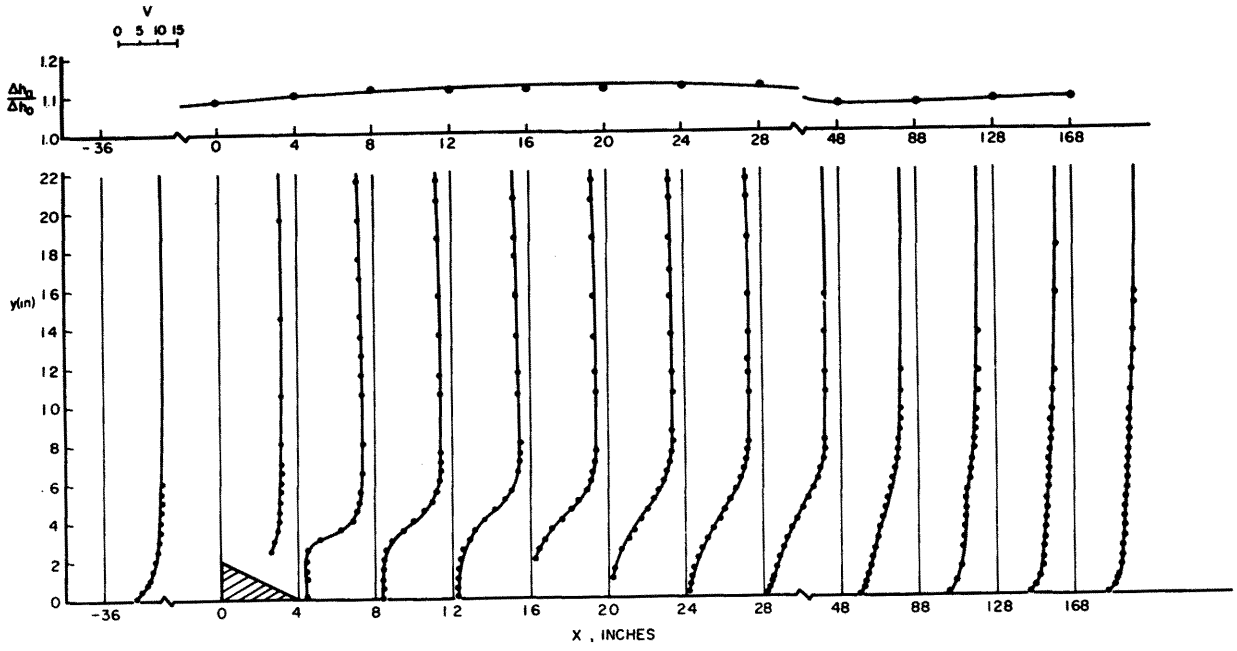

FIG.19 VELOCITY DISTRIBUTION FOR 2"x 4" HILL , SMALL WIND TUNNEL $u_o \sim 15$ fps.

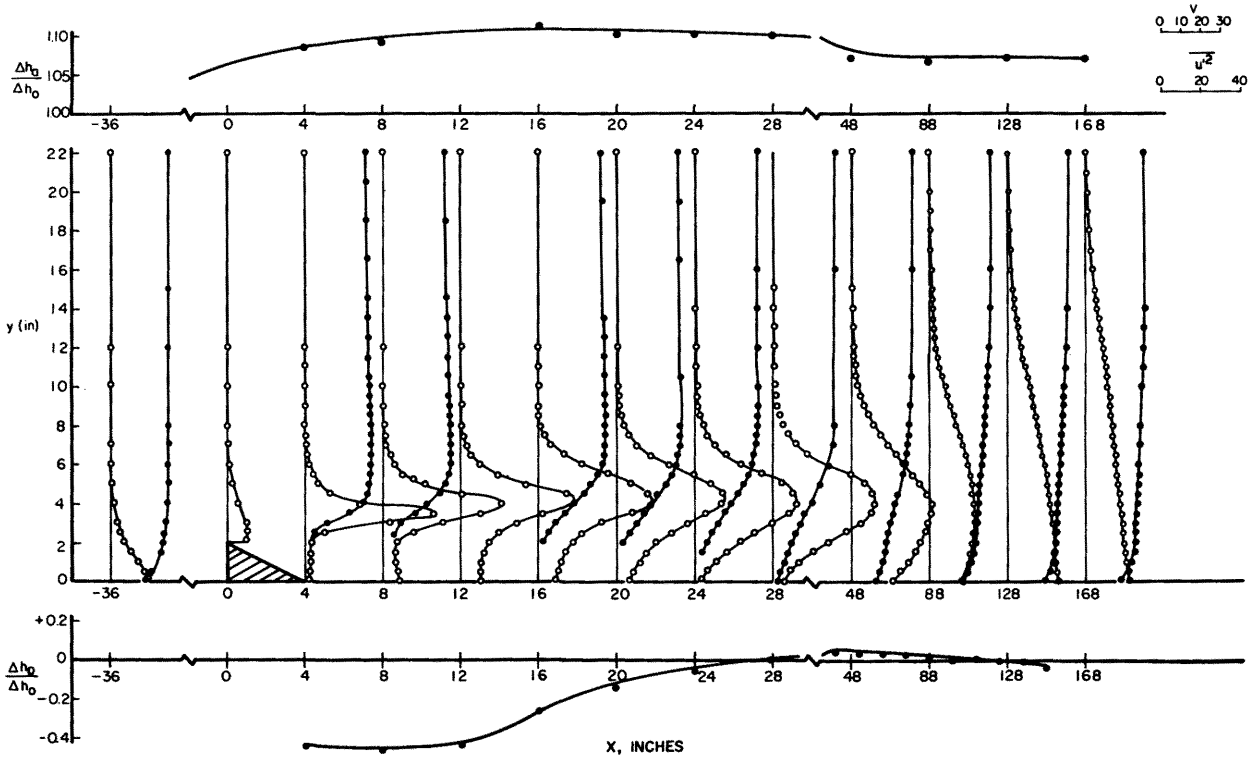

FIG. 20 VELOCITY DISTRIBUTION FOR 2"x 4" HILL, SMALL WIND TUNNEL $u_o \sim 30$ fps.

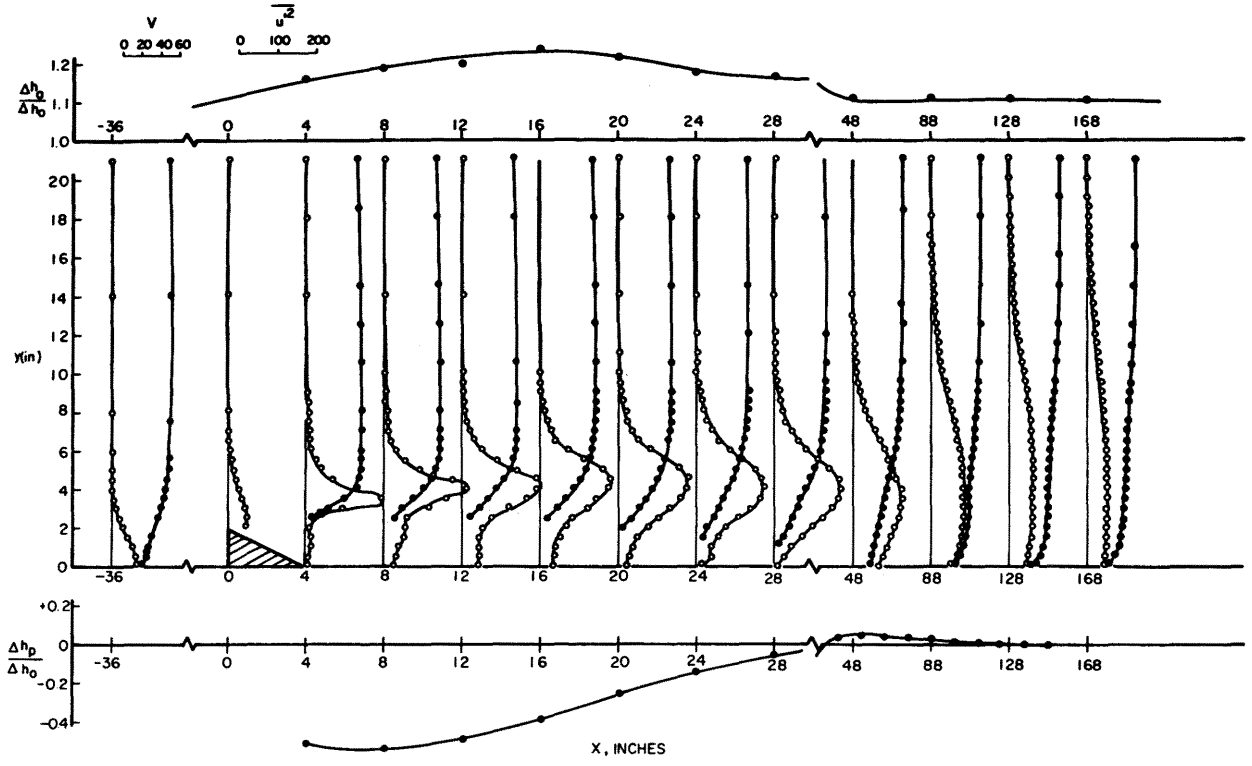

FIG.21 VELOCITY DISTRIBUTION FOR 2"x 4" HILL, SMALL WIND TUNNEL u_0 = 60 fps.

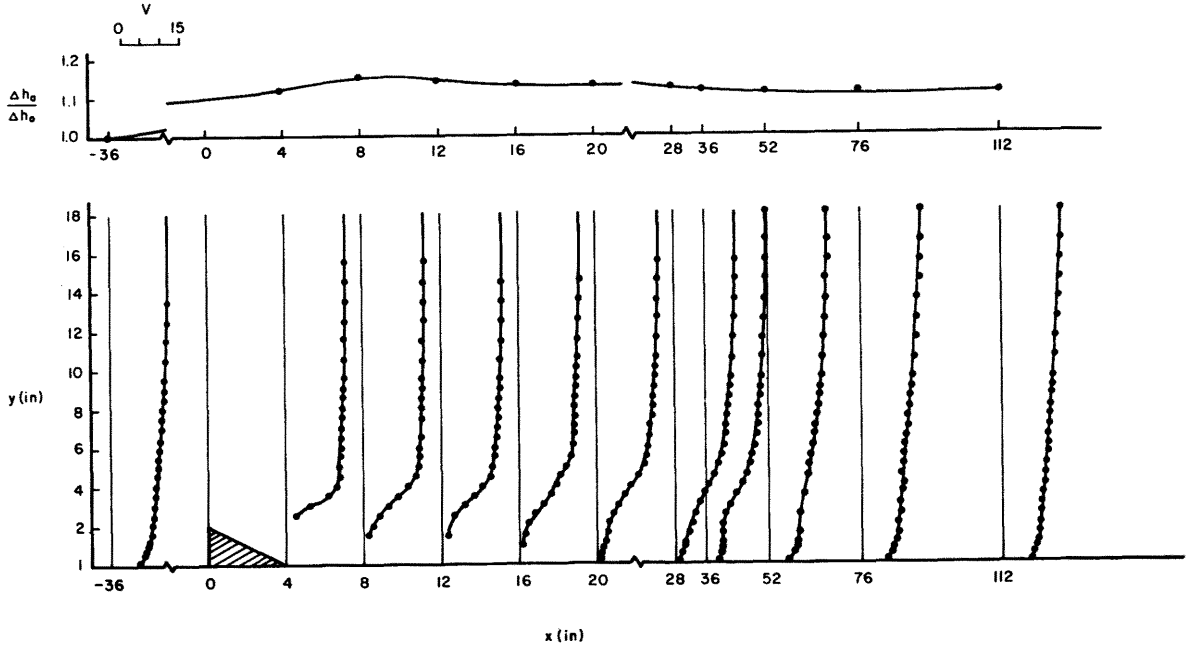

FIG. 22 VELOCITY DISTRIBUTION FOR 2"x 4" HILL, BIG WIND TUNNEL $u_0 \sim 15$ fps.

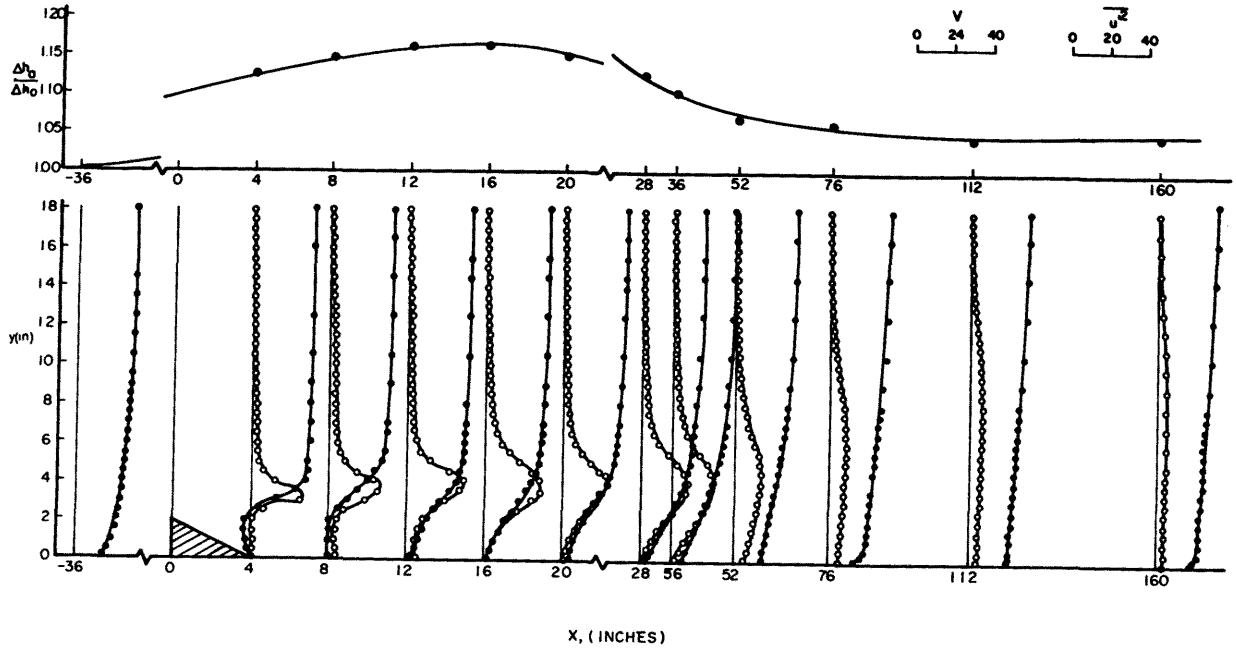

FIG. 23 VELOCITY DISTRIBUTION FOR 2"x4" HILL, BIG WIND TUNNEL $u_0 \sim 30$ fps.

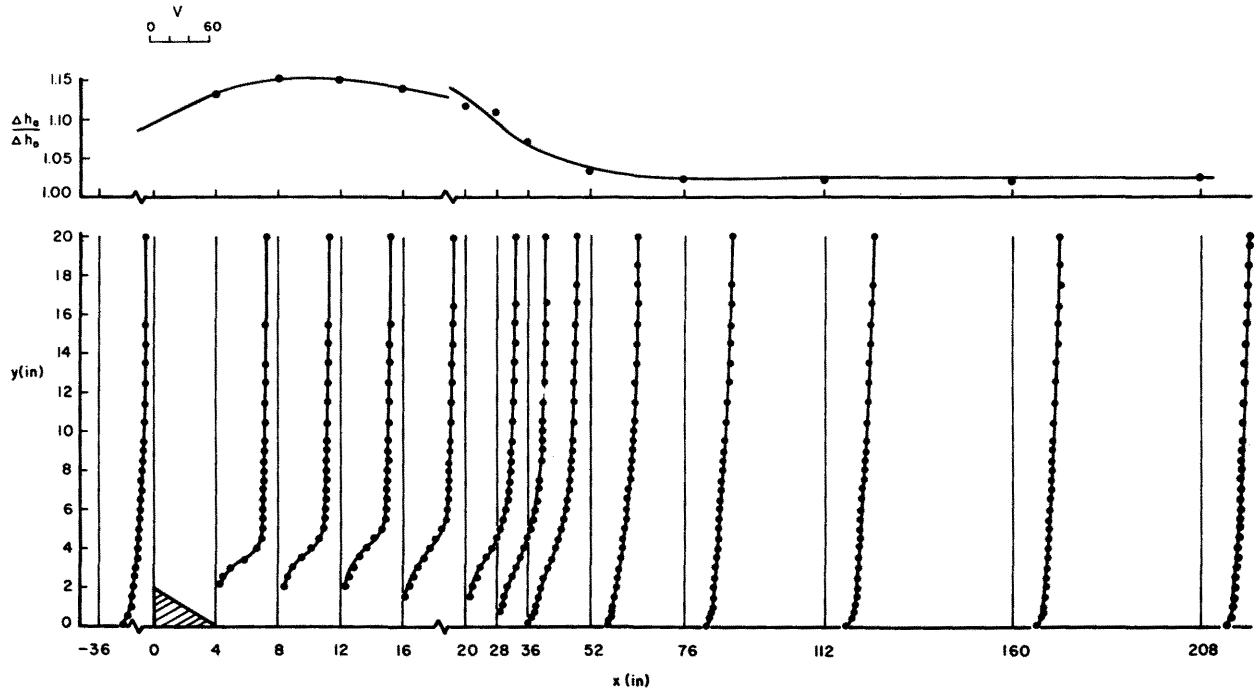

FIG. 24 VELOCITY DISTRIBUTION FOR 2"x 4" HILL, BIG WIND TUNNEL $u_0 \sim 60$ fps.

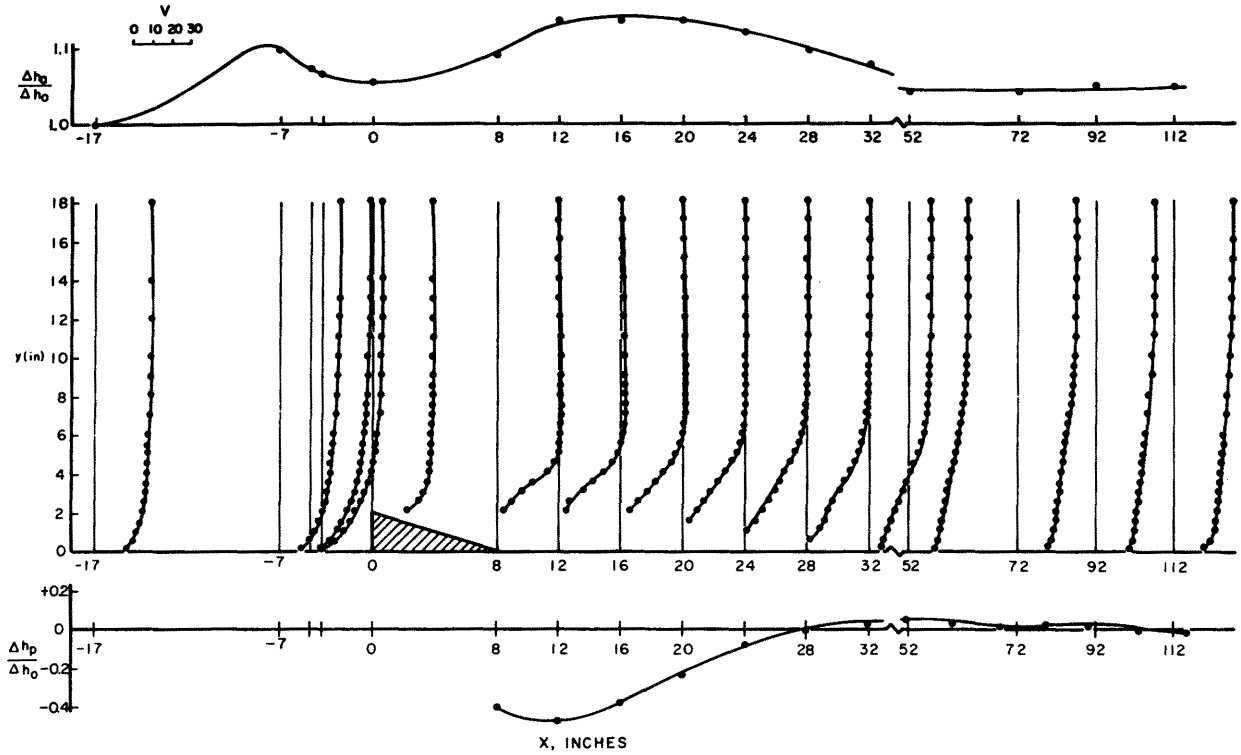

FIG. 25 VELOCITY DISTRIBUTION FOR 2"x 8" HILL, SMALL WIND TUNNEL $u_0 \sim 30$ fps.

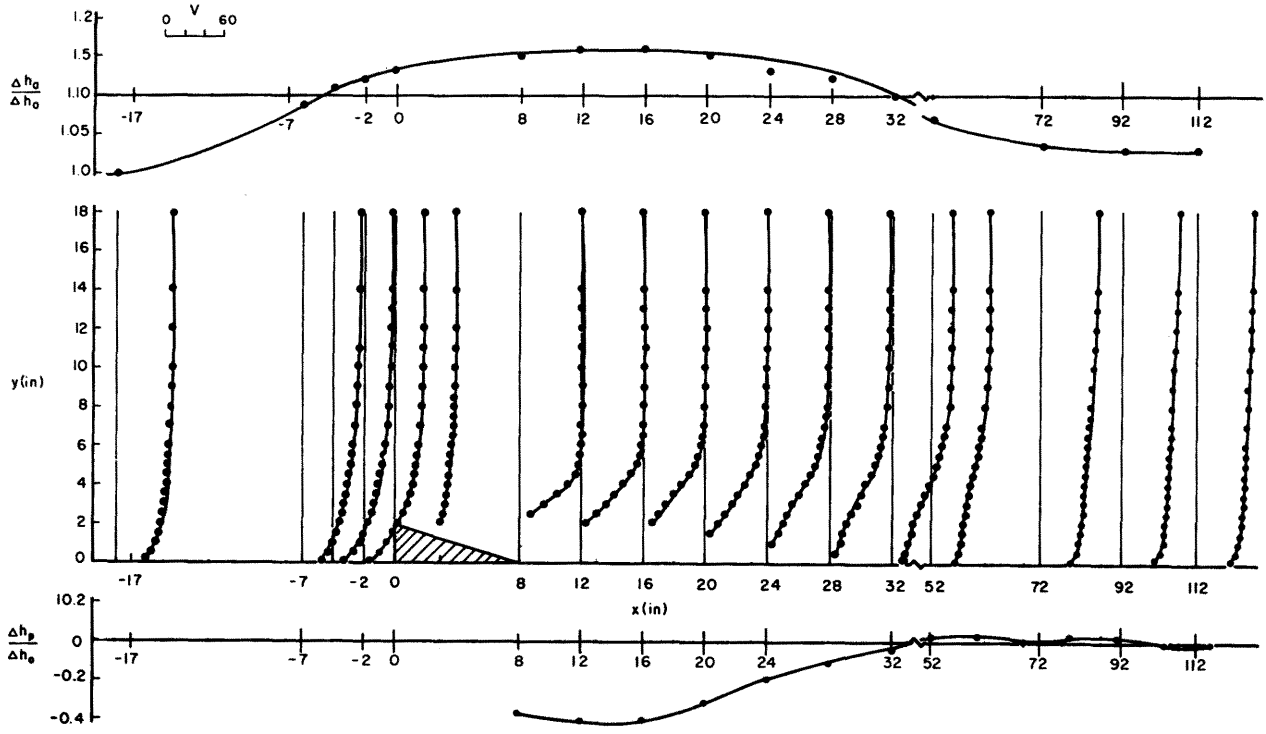

FIG. 26 VELOCITY DISTRIBUTION FOR 2"x 8", SMALL WIND TUNNEL $u_0 \sim 60$ fps

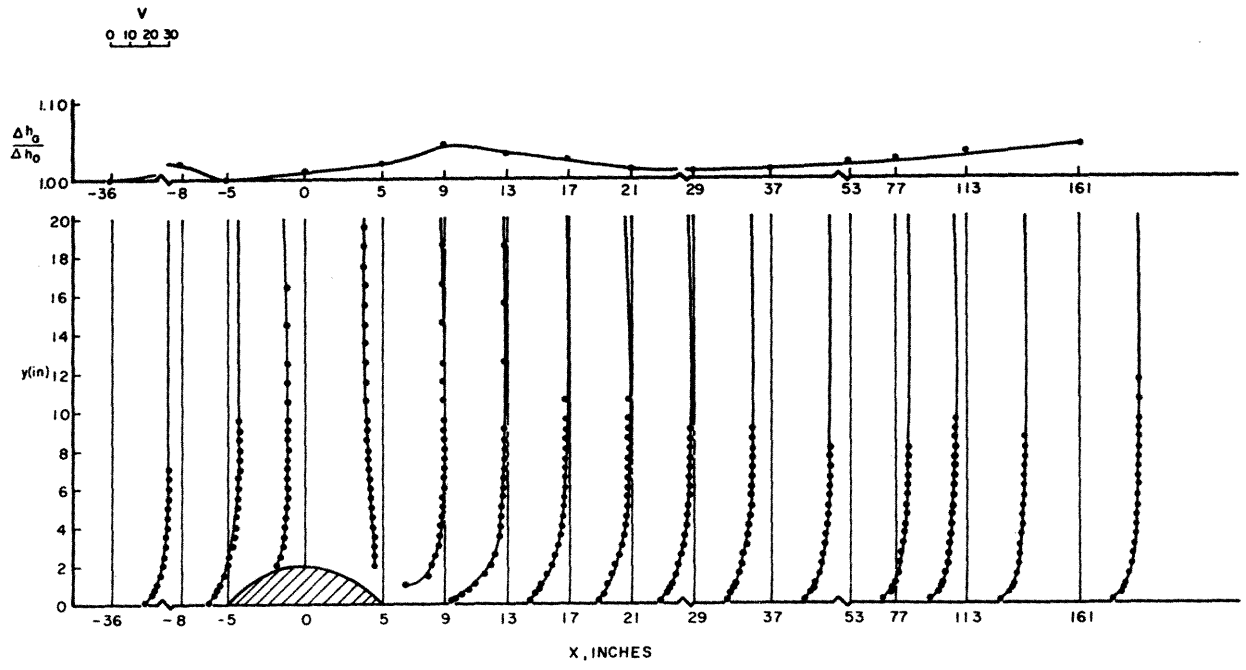

FIG. 27 VELOCITY DISTRIBUTION FOR 2" x 10" SMALL WIND TUNNEL u_0~30 fps

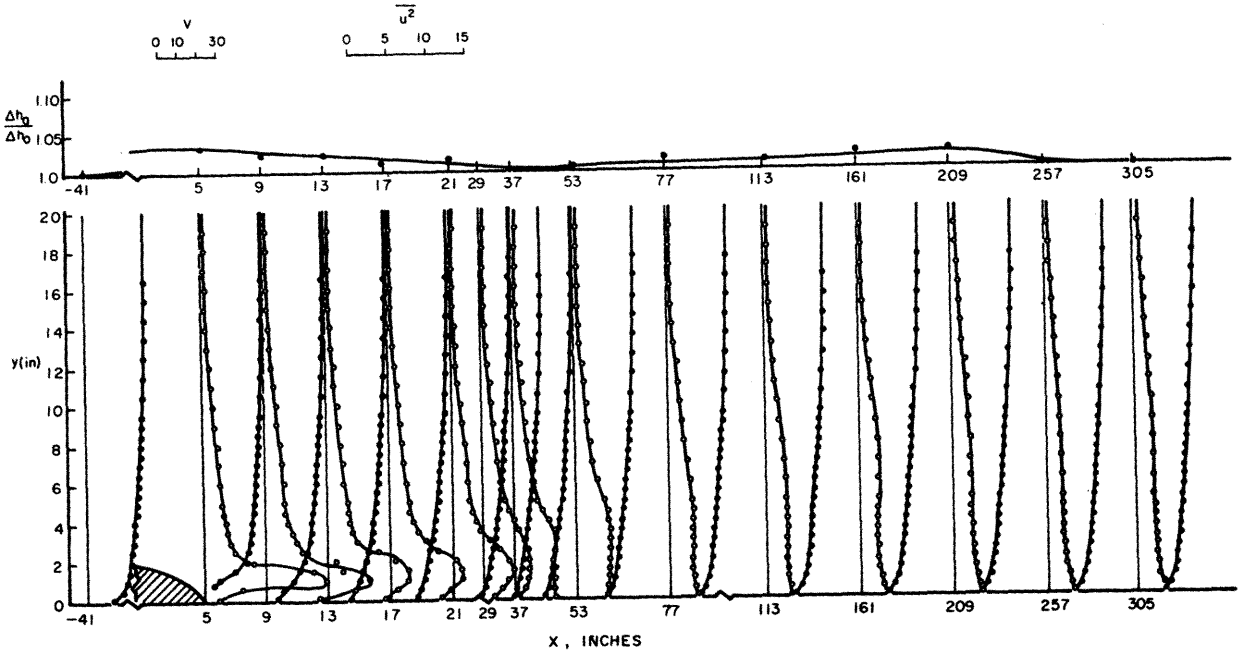

FIG. 28 VELOCITY DISTRIBUTION FOR 2"x 10" HILL, BIG WIND TUNNEL u_0~30 fps.

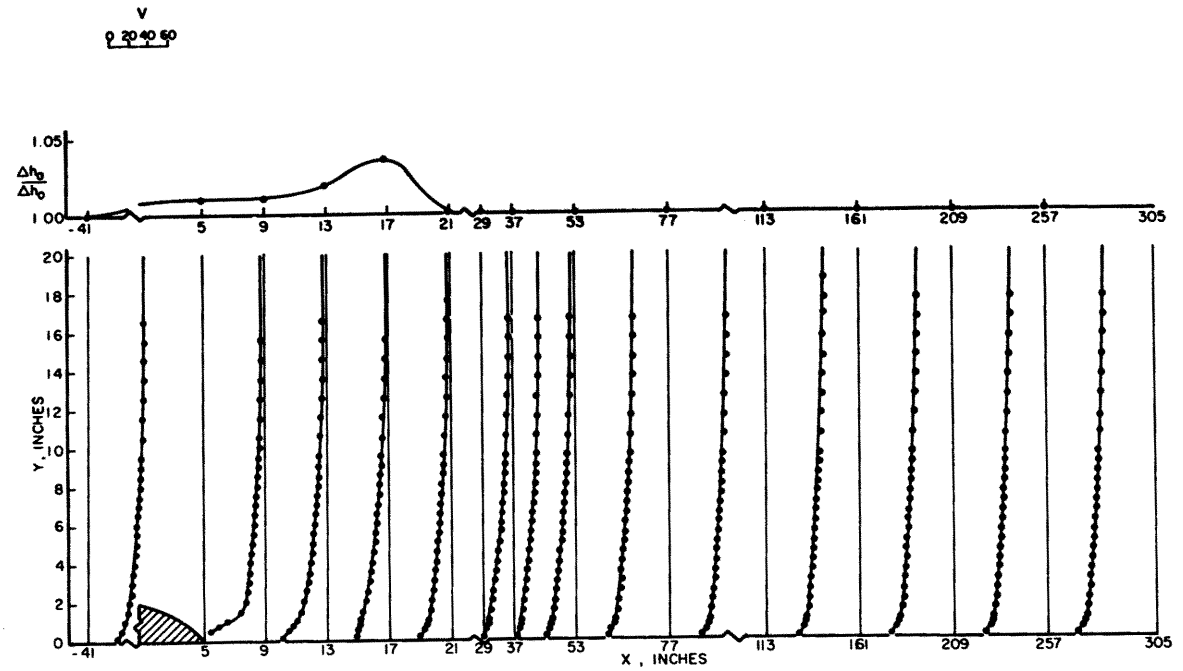

FIG. 29 VELOCITY DISTRIBUTION FOR 2" x 10" HILL, BIG WIND TUNNEL $u_o \sim 60$ fps.

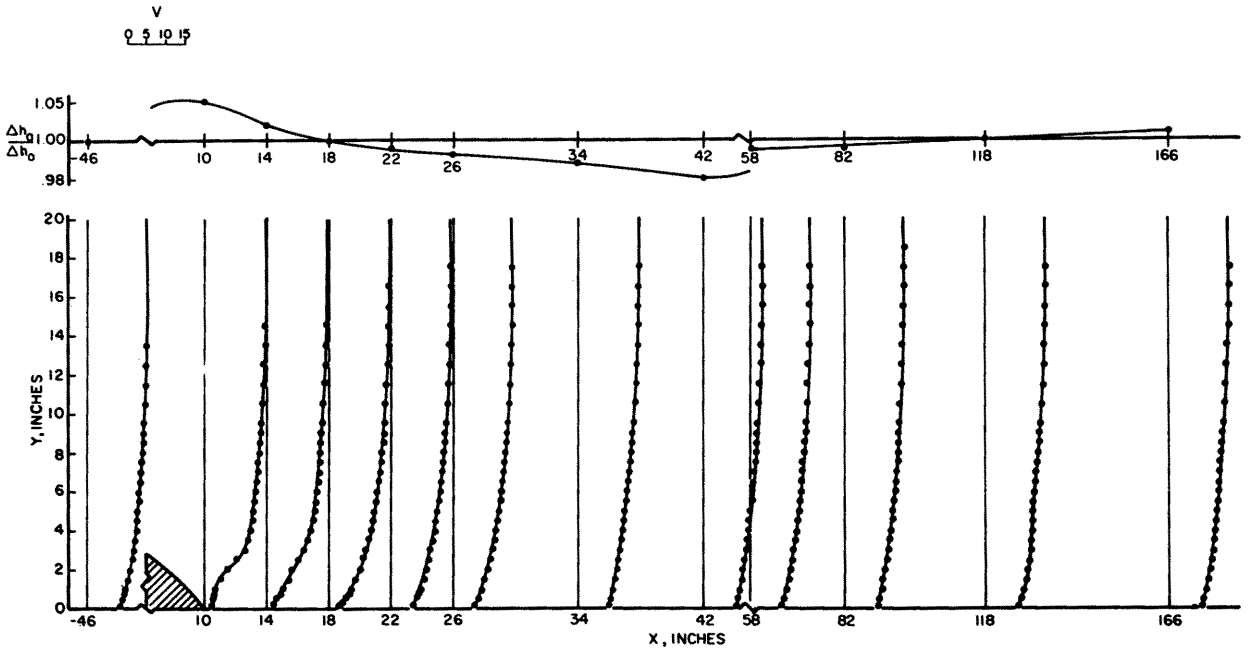

FIG. 30 VELOCITY DISTRIBUTION FOR 4"x 20" HILL, BIG WIND TUNNEL $u_o \sim 15$ fps

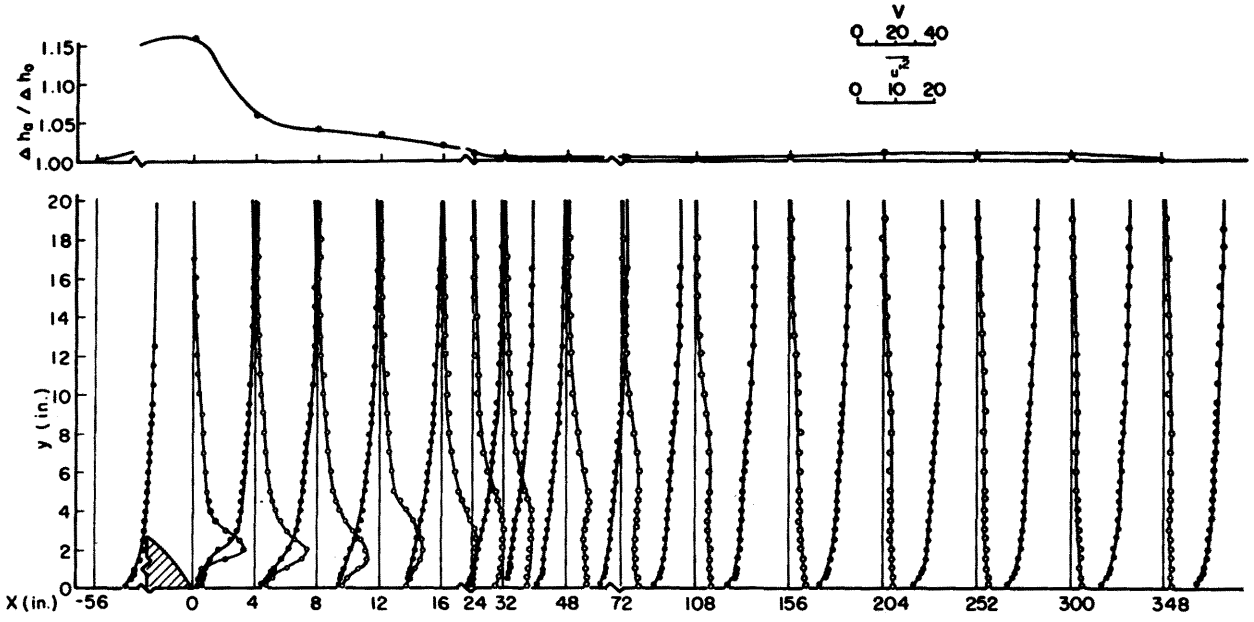

FIG. 31 VELOCITY DISTRIBUTION FOR 4" x 20" HILL, BIG WIND TUNNEL u_0~30 fps

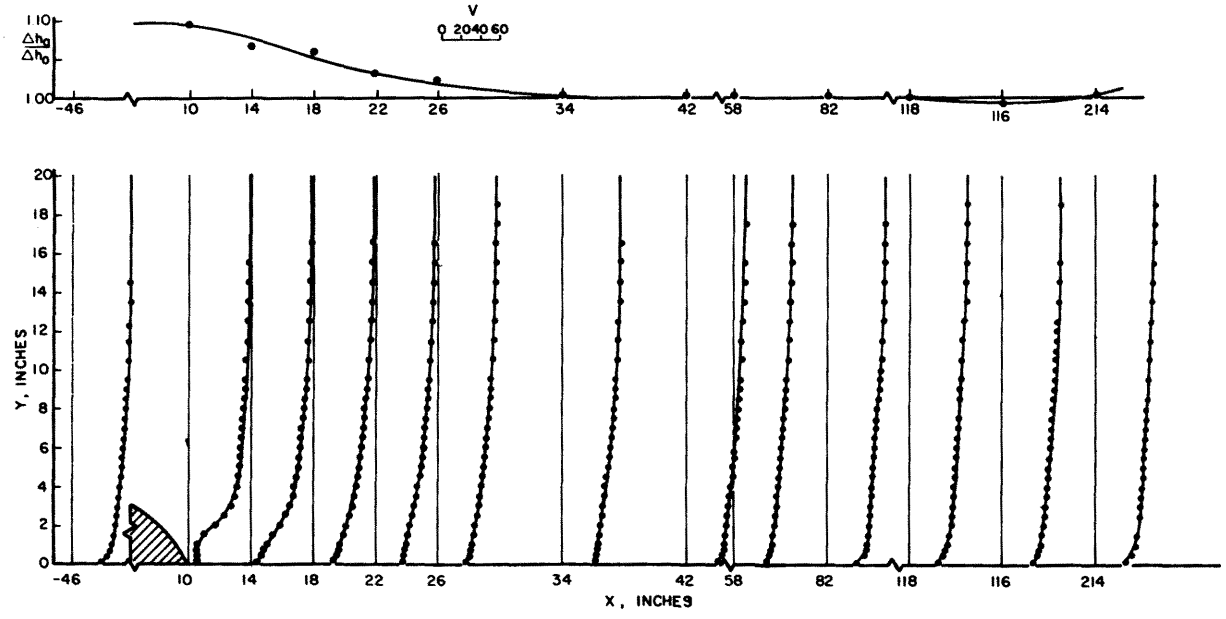

FIG. 32 VELOCITY DISTRIBUTION FOR 4" x 20" HILL, BIG WIND TUNNEL $u_0 \sim 60$ fps.

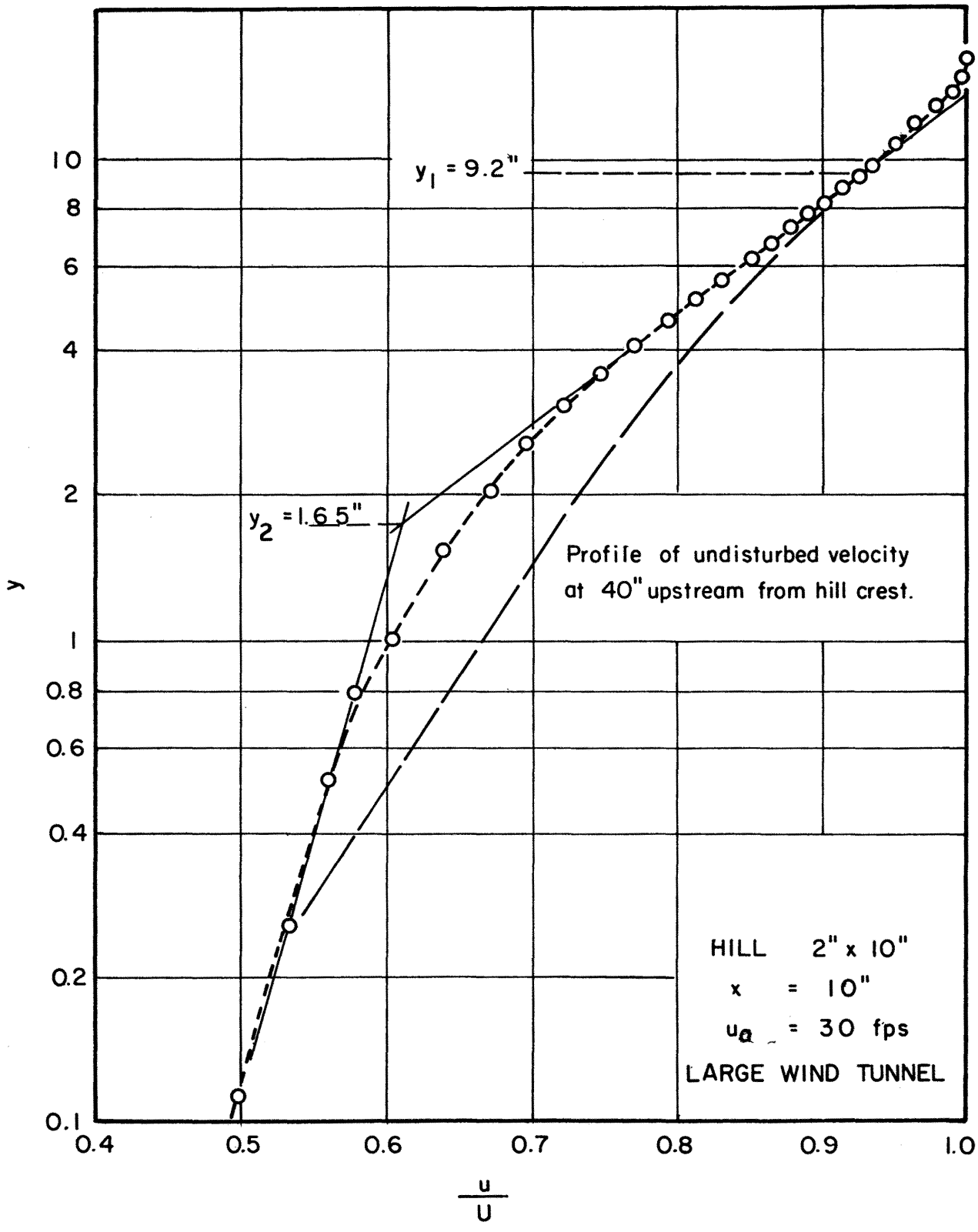

FIG. 36 EXAMPLE OF DETERMINING THE SUBLAYERS

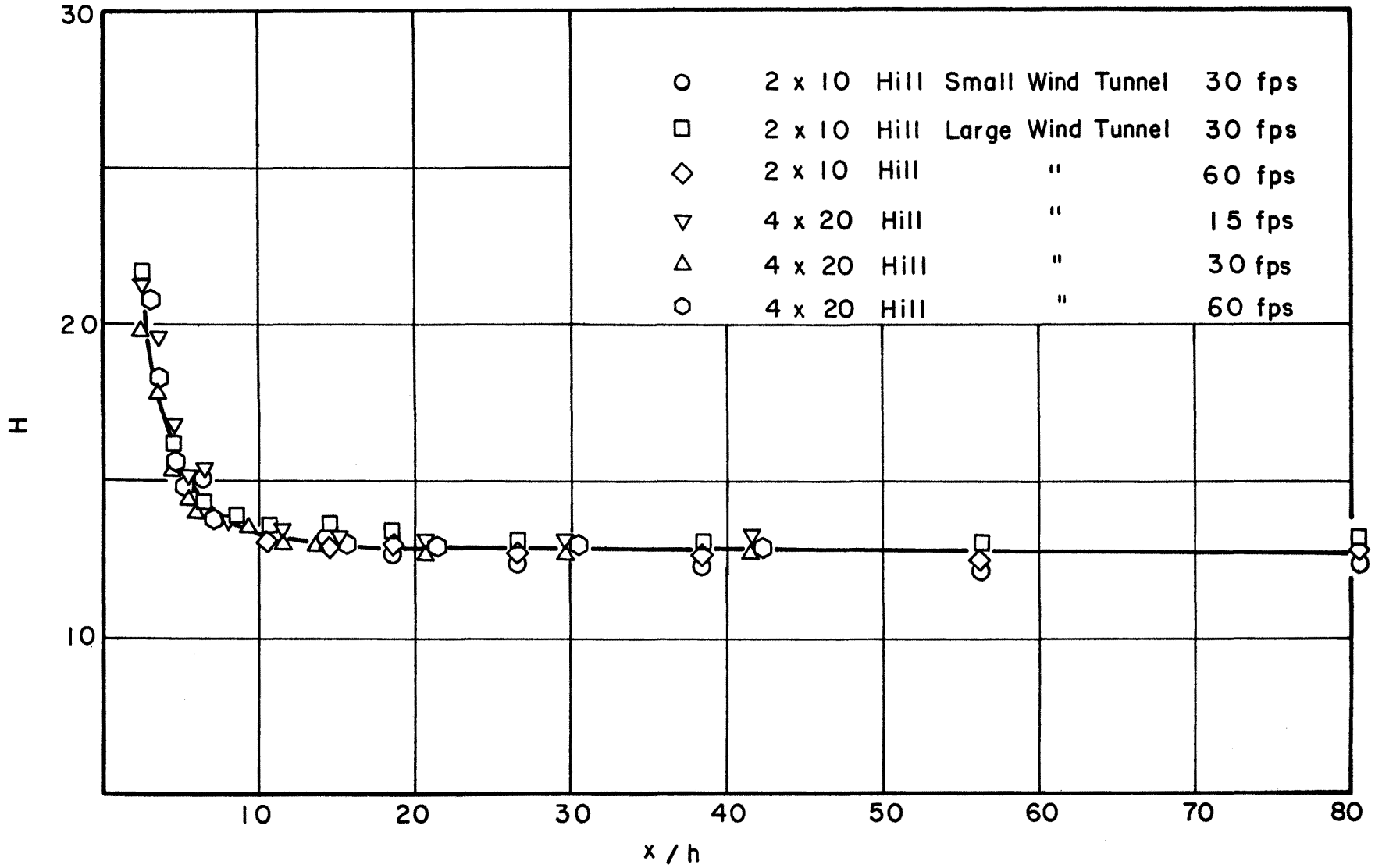

FIG. 37 SHAPE FACTOR H FOR SINUSOIDAL HILLS

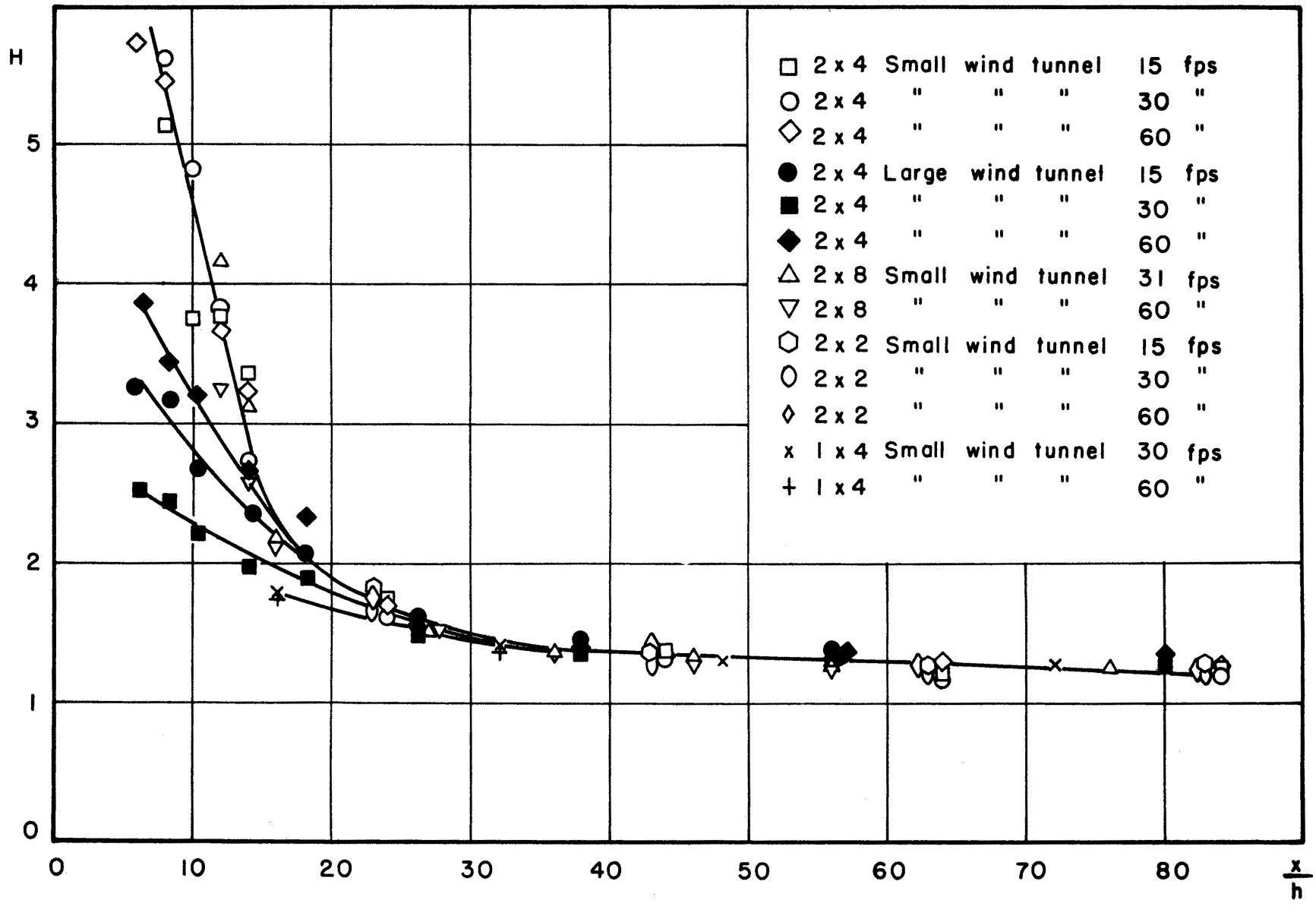

FIG. 38 SHAPE FACTOR H FOR WEDGE SHAPED HILLS

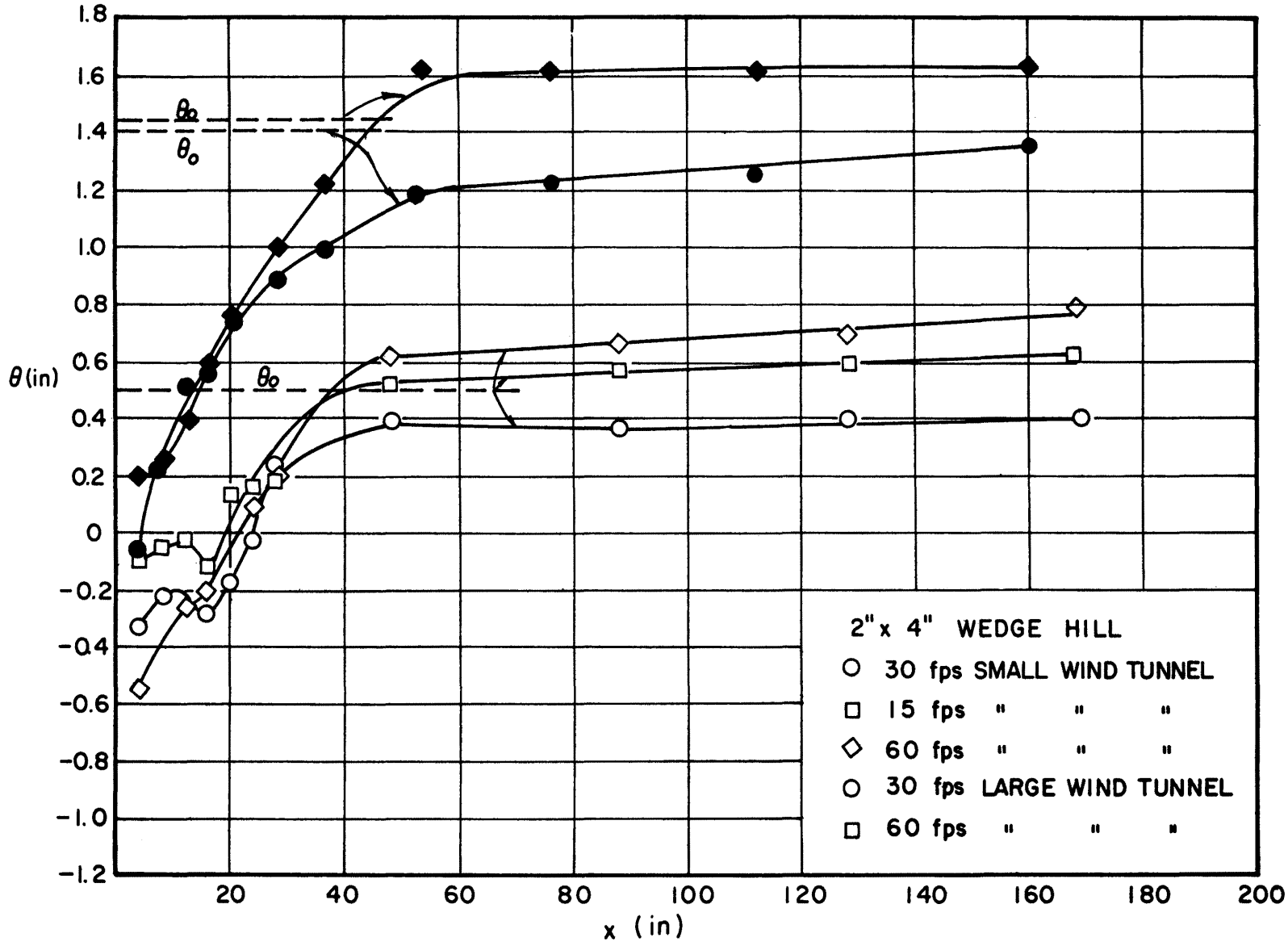

FIG. 39 MOMENTUM BALANCE FOR DETERMINING x_3

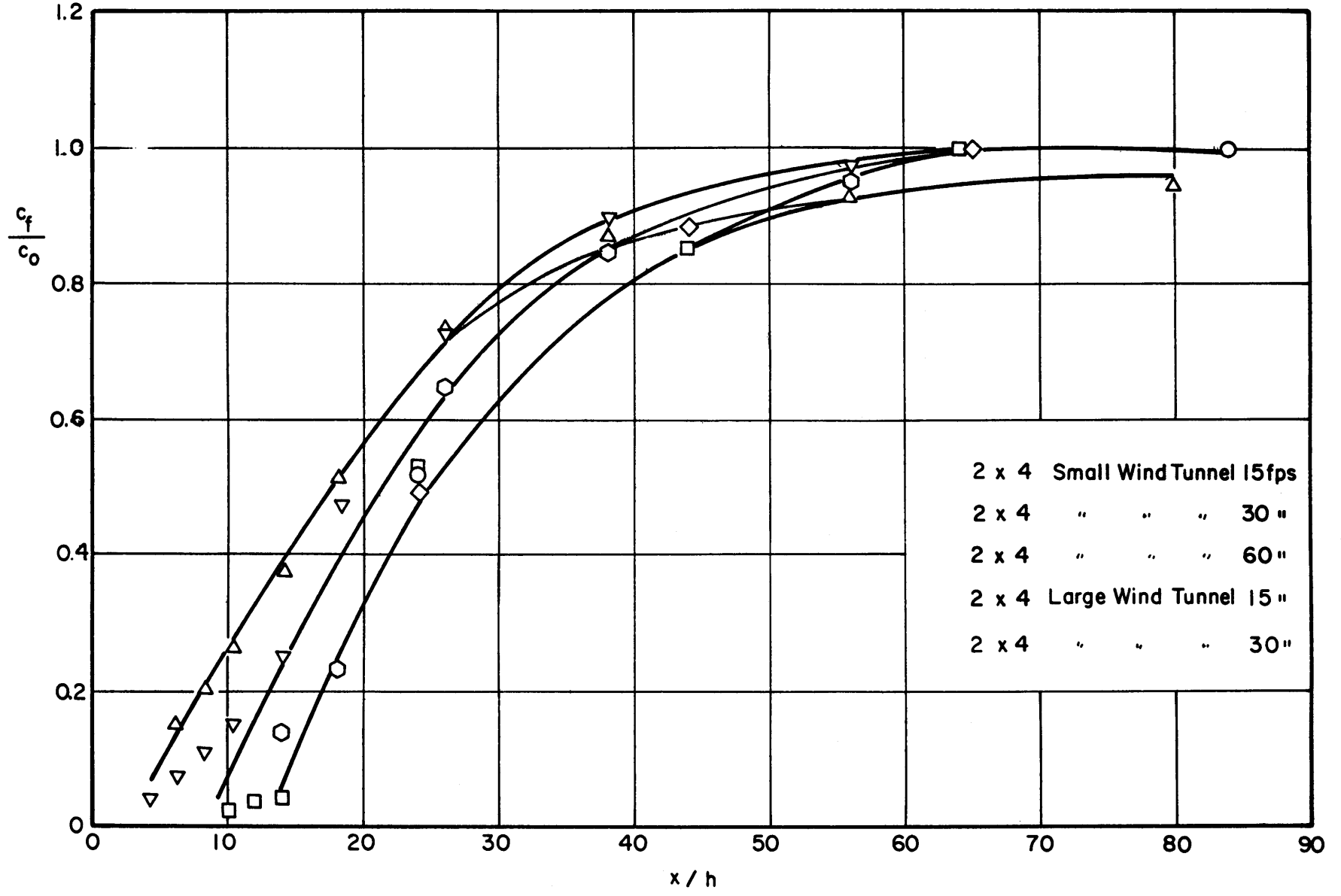

FIG. 40 SHEAR STRESS COEFFICIENT c_f / c_o FOR 2"x 4" WEDGE HILL

① UNDISTURBED BOUNDARY LAYER (OUTER LAYER)

② REGION OF HILL INFLUENCE (MIDDLE LAYER)

③ REGION OF REESTABLISHING BOUNDARY LAYER (INNER LAYER)

④ BLENDING REGION BETWEEN MIDDLE AND OUTER LAYER

⑤ BLENDING REGION BETWEEN INNER AND MIDDLE LAYER

⑥ STANDING EDDY ZONE

⑦ POTENTIAL OUTER FLOW

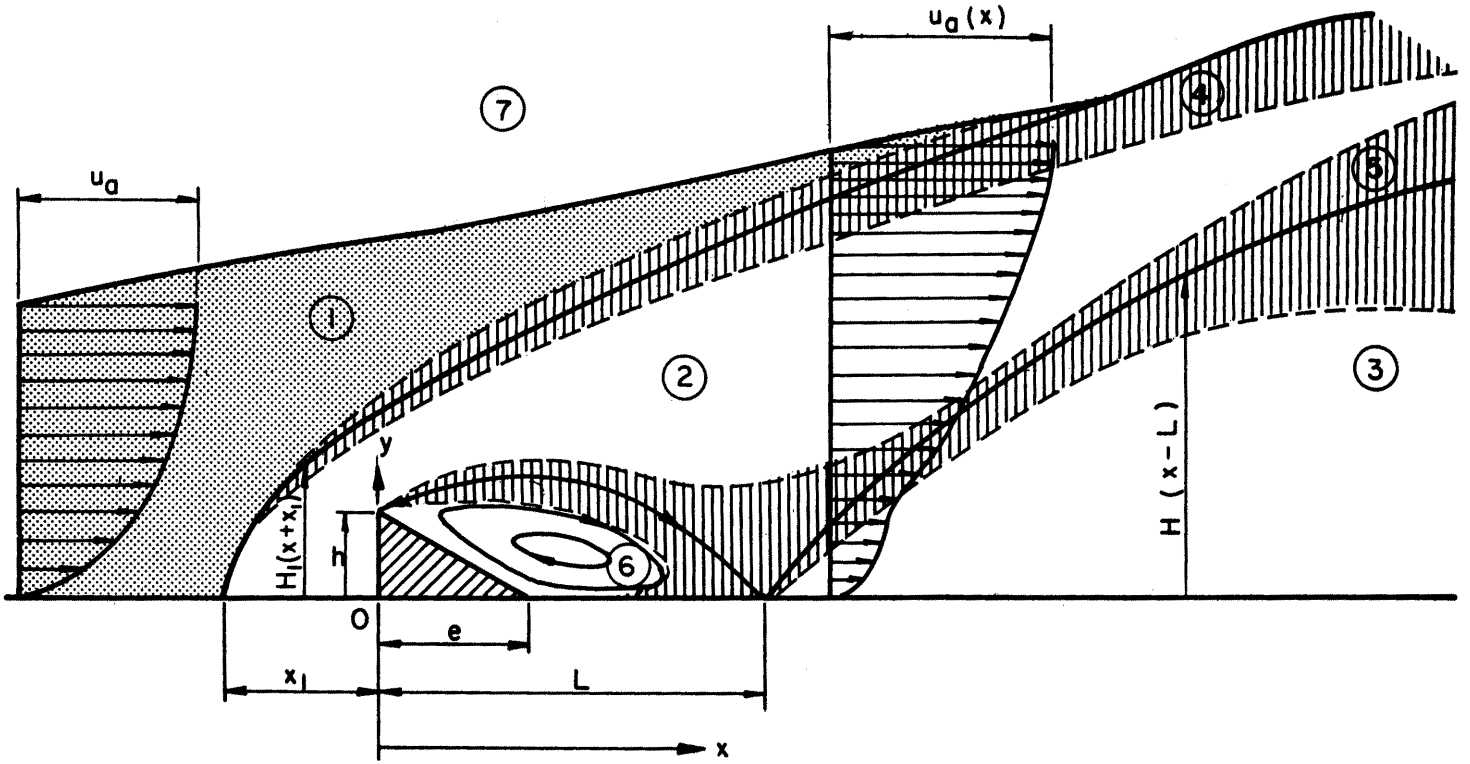

FIG. 41 DEFINITION OF FLOW ZONES

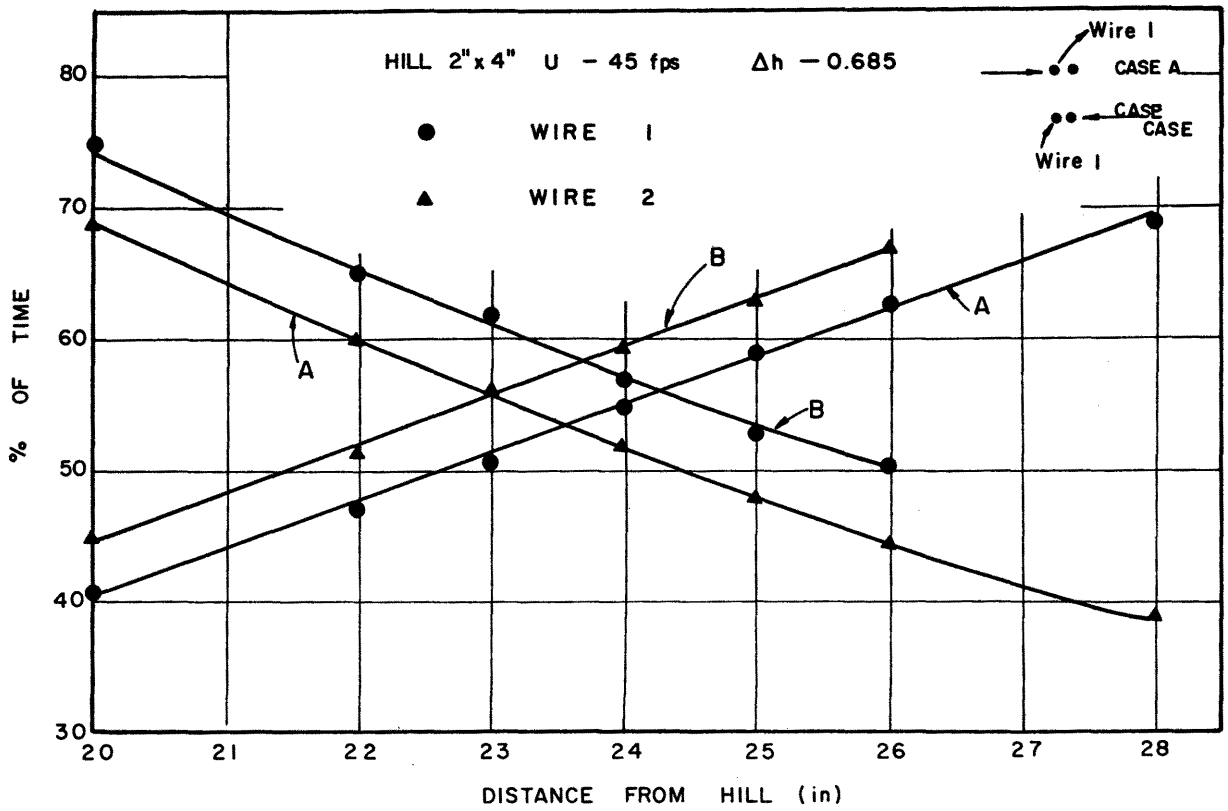

FIG. 42 EXAMPLE OF DETERMINATION OF L

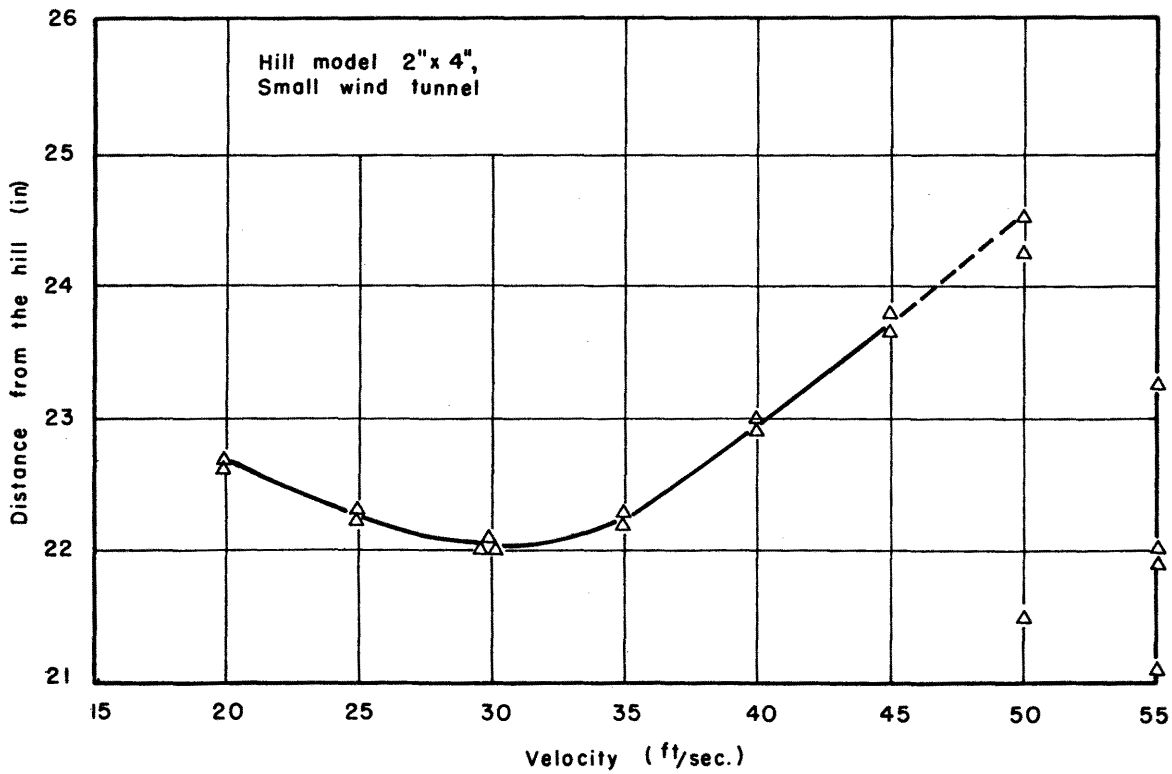

FIG. 43 DETERMINATION OF THE DISTANCE L

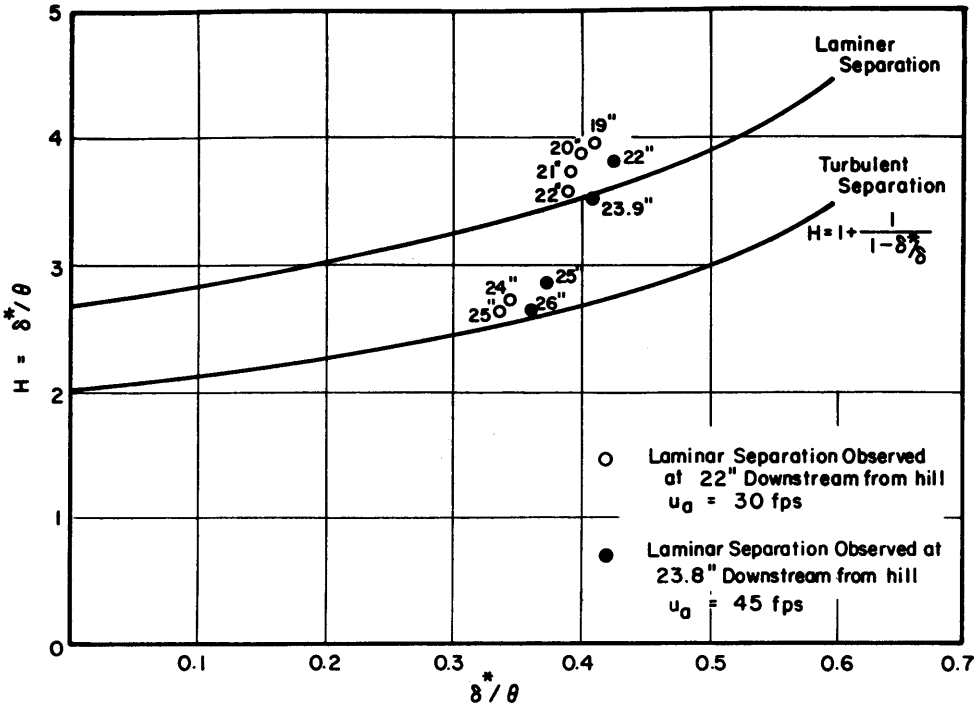

FIG. 44 HILL 2" x 4" SEPARATION CRITERION

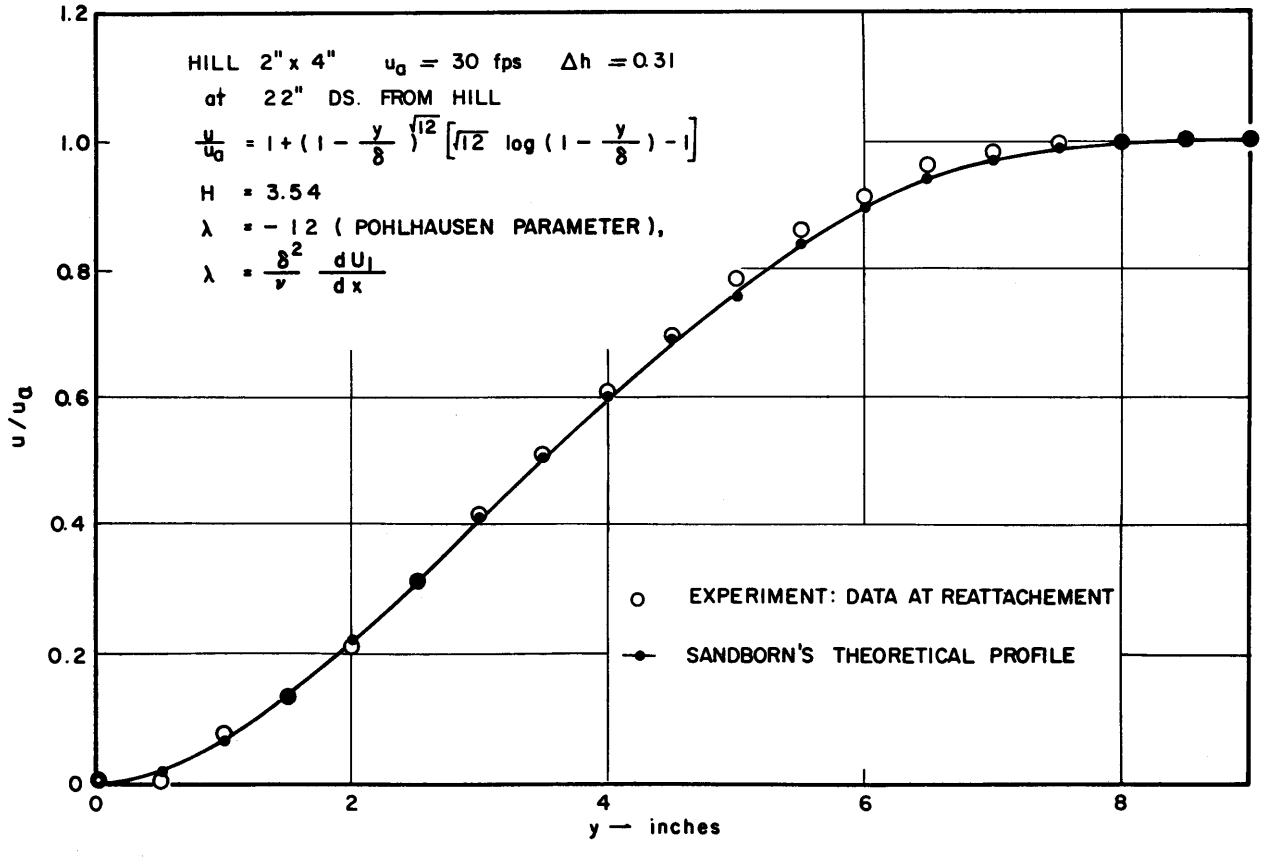

FIG. 45 CALCULATED VELOCITY PROFILE AT REATTACHEMENT

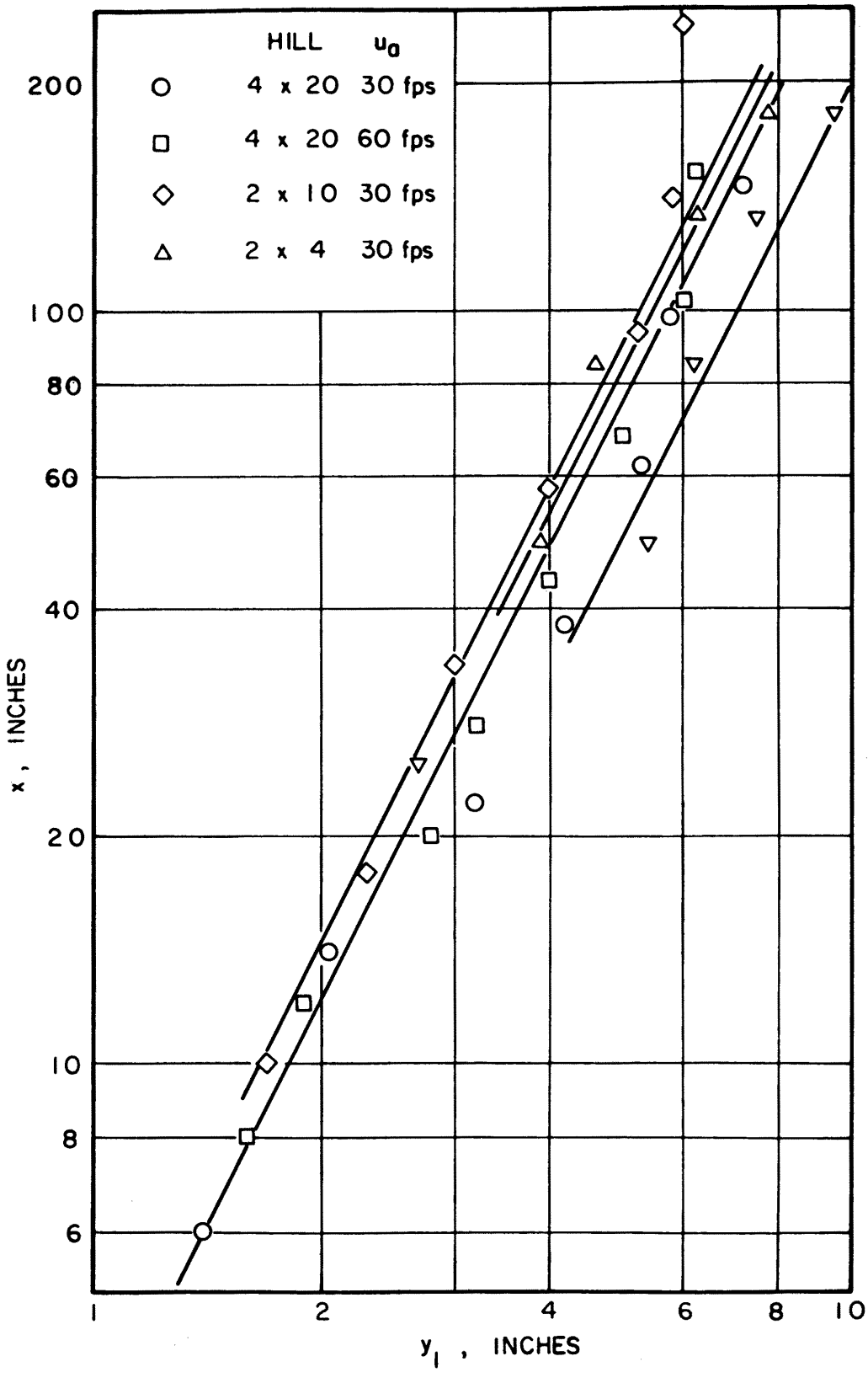

FIG. 46 THE BOUNDARY OF THE INNER LAYER

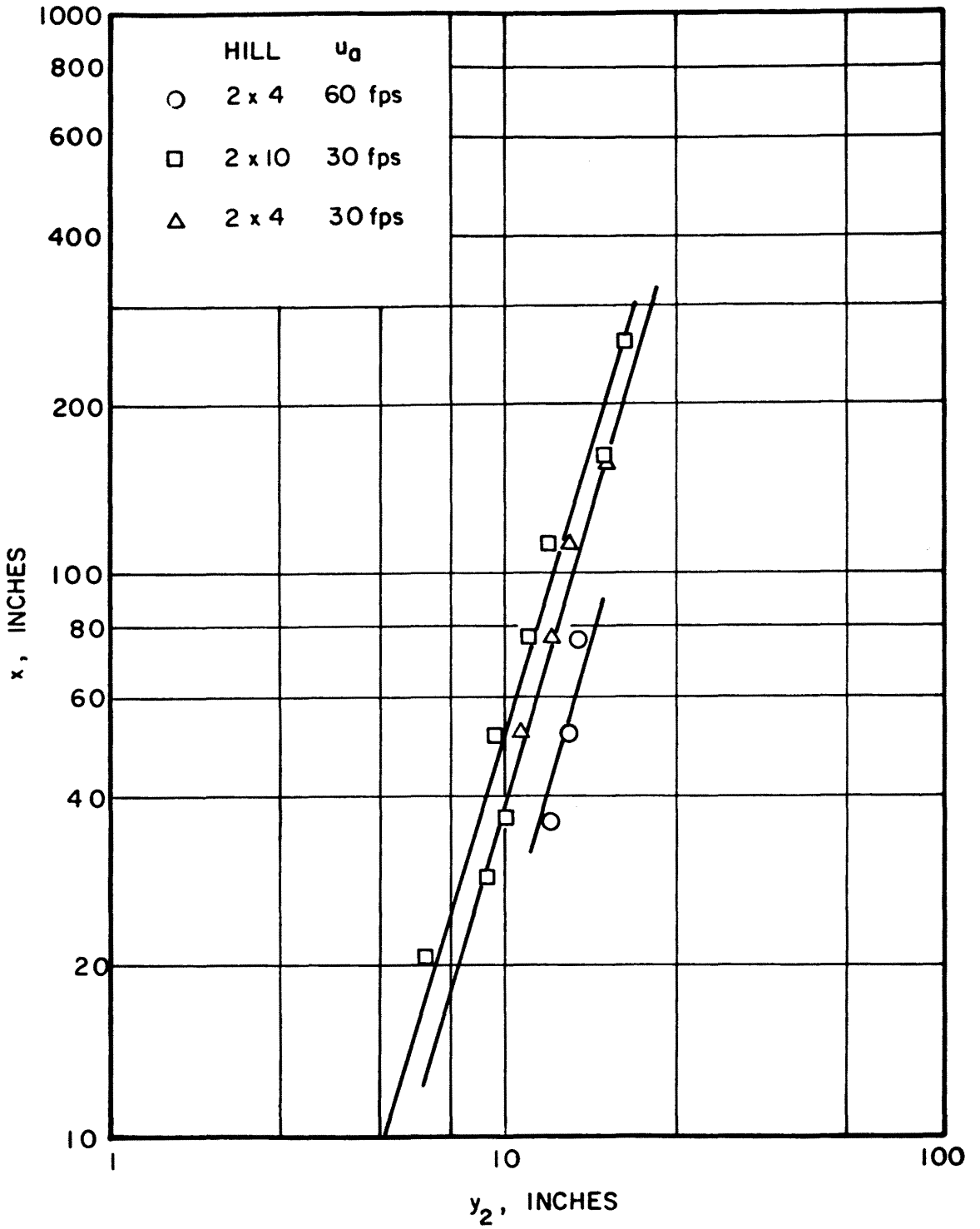

FIG. 47 THE DISTANCE OF THE OUTER BOUNDARY FROM THE WALL

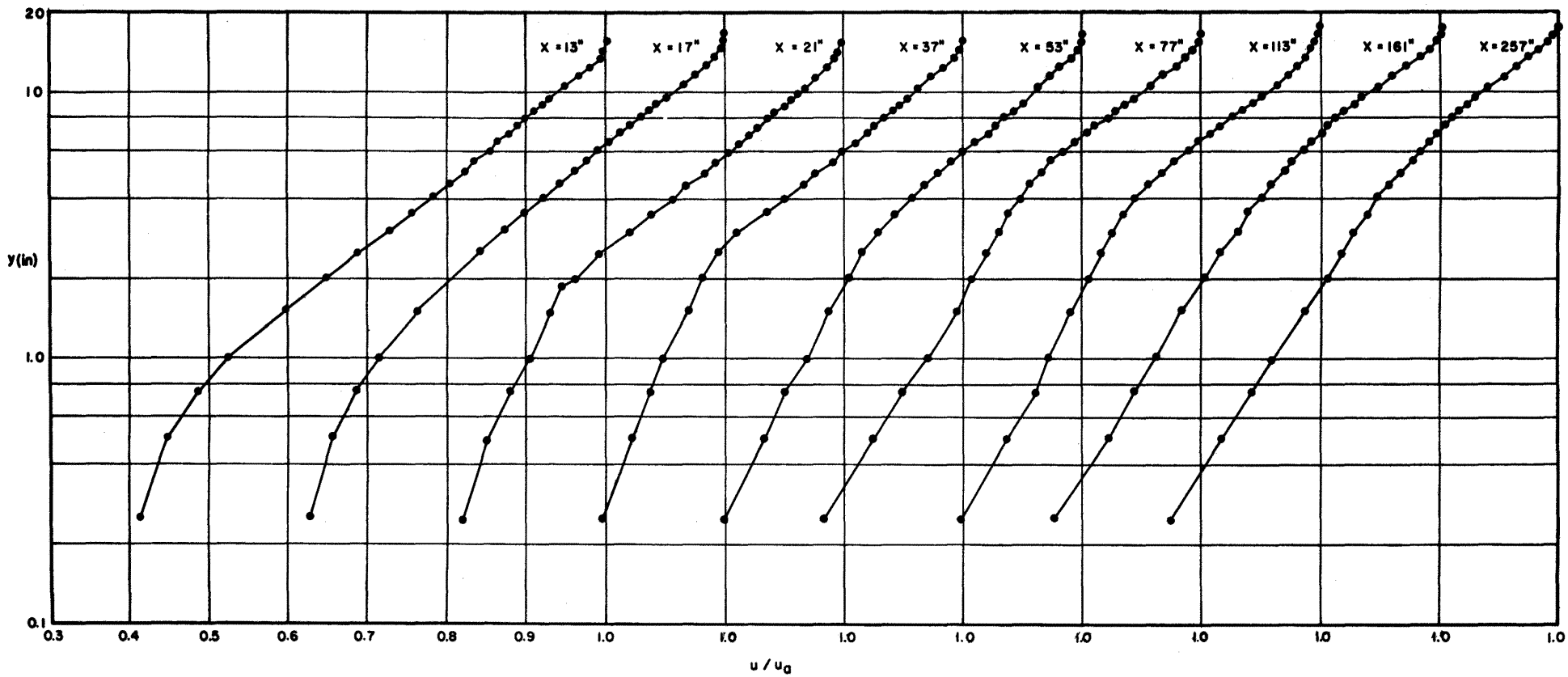

FIG. 48 EXAMPLES OF NONDIMENSIONAL VELOCITY PROFILES FOR u_a = 30 fps

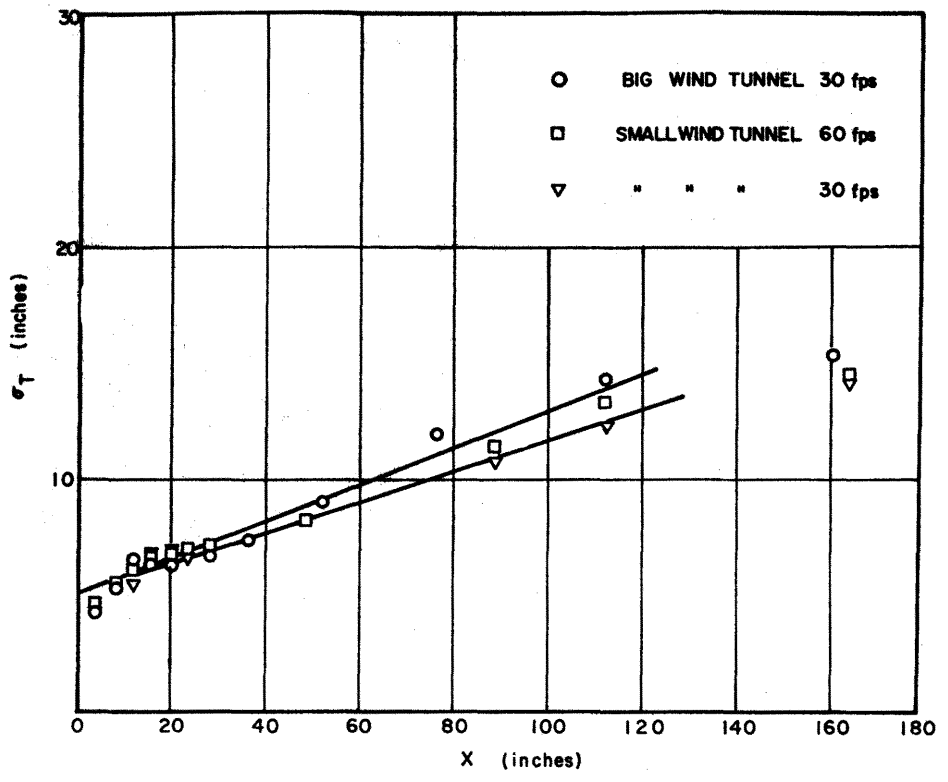

FIG. 49 σ_T AS FUNCTION OF x FOR 2" x 4" WEDGE WEDGE

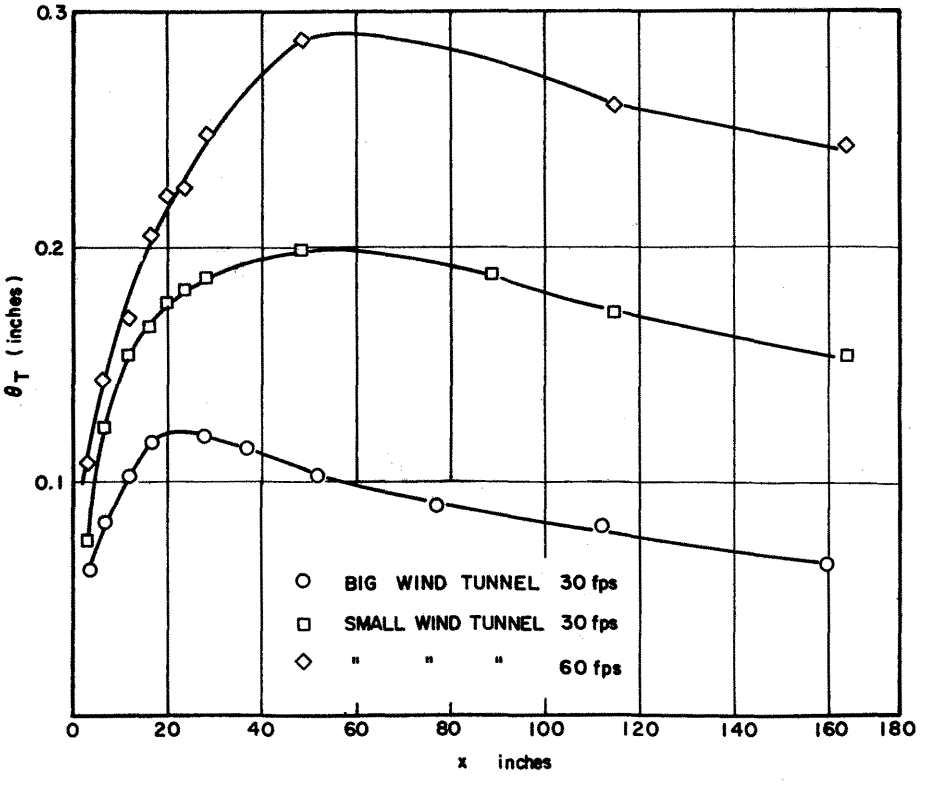

FIG. 50 θ_T AS FUNCTION OF x FOR 2" x 4" WEDGE

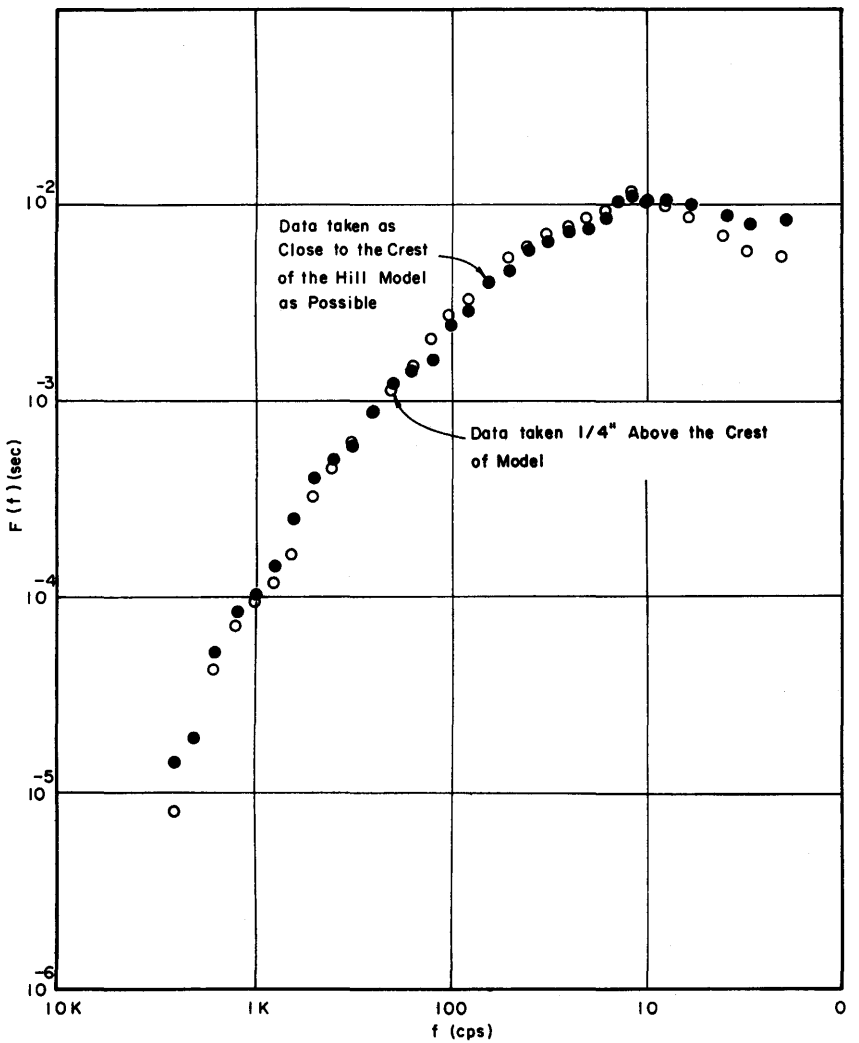

FIG. 51 TURBULENT INTENSITY SPECTRA NEAR THE CREST OF A SINUSOIDAL MODEL HILL

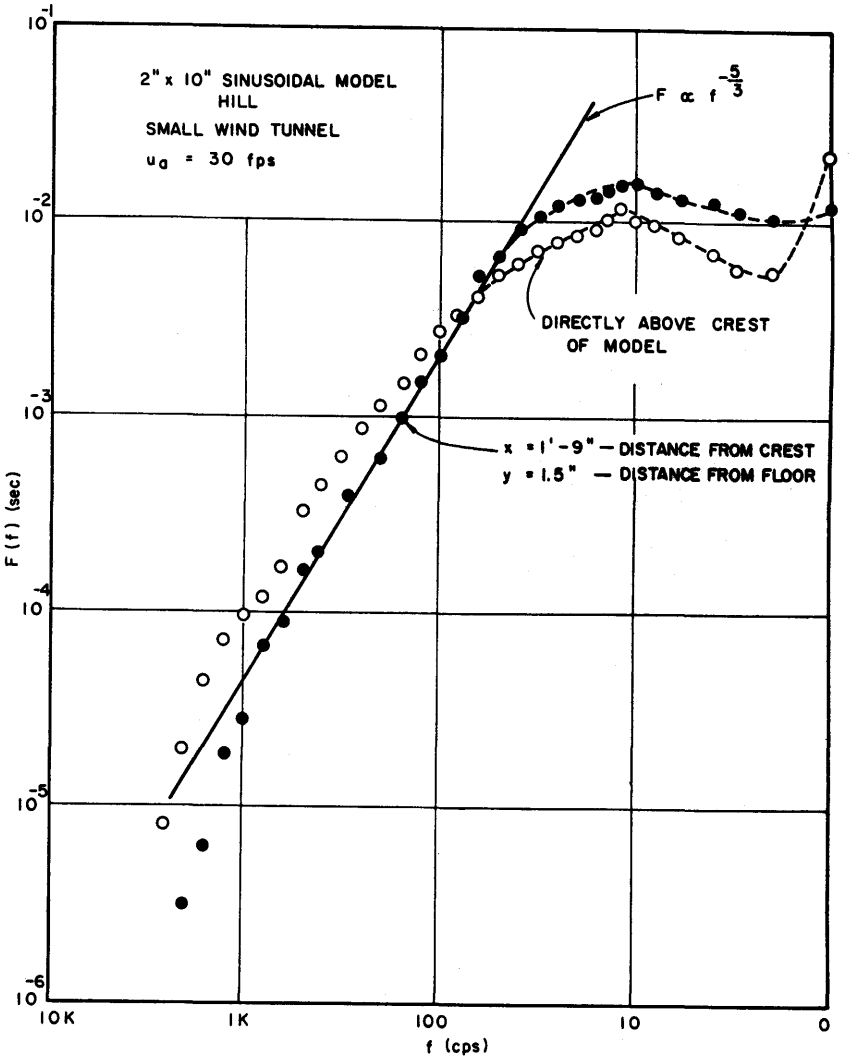

FIG. 52 COMPARISON OF TURBULENCE SPECTRA FOR SINUSOIDAL MODEL HILL